Modeling of 2D Cylindrical Integrated Optical Microresonators

K. R. (Kiran) Hiremath

Supervised by,
Dr. Manfred Hammer

June 13, 2003

Abstract

In this thesis, we discuss the modeling and simulation of 2D cylindrical integrated optical microresonator based on spatial couple mode theory. A symmetric dual coupling microresonator device is functionally decomposed into two couplers each one consisting of a straight waveguide and a bent waveguide. These two couplers are internally connected to each other by two other bent waveguides. Each coupler is externally connected to two other straight waveguides. The advantage of such decomposition is that the modeling of the microresonator reduces to the modeling of a bent waveguide and the modeling of the coupler involving a bent waveguide and a straight waveguide. For this, it is essential to know the bent modes. We present the modeling of bent waveguide and developed the semi analytical bent mode solver. We use these modes in the spatial couple mode theory based modeling of the coupler involving a bent and a straight waveguide. The scattering matrix of this coupler plays important role in the modeling of a microresonator. Then we present the model of microresonator which is completely characterised by the coupler scattering matrix. We conclude the modeling of a microresonator with the simulation results.

Contents

Chapter 1

Introduction

The optical fiber brought advantages of optics to the walls of houses. The next step is to use optics directly in different appliances. In today's ICT market, cost of a device determines the acceptance of new technology. Integrated Circuit technology showed that cost can be reduced, while increasing the complexity and functionality of a device without compromising reliability.

Recent advances in the fabrication technology enabled compact, high finesse and picosecond cavity lifetime microresonators(MRs). This device can be used as a laser [36], optical switch [6], multiplexer, filter [7, 38] or as a logic gate. We are interested in a MR as a tunable channel dropping filter that selects one specific channel of a wavelength division multiplexed signal without disturbing other channels. Due to its superior functionality to select a single channel with a very narrow linewidth, compactness and the possibility of dense integration, a MR is an attractive add/drop wavelength filter.

1.1 Microresonators

Typically a microresonator consists of two parallel dielectric waveguides which are evanescently coupled to a cylindrical/disc/ring shaped cavity, as shown in figure 1.1. A signal is launched in the *In* port waveguide. It excites the modes of the cylindrical cavity. Part of the input signal gets coupled to the cylindrical cavity and the remaining signal appears at the *Through* port. In turn, part of it gets coupled to the *Drop* port waveguide. Depending upon given structural parameters, at resonance frequency all input power appears at the *Drop* port. But in practice, due to the radiation losses in cylindrical cavity, the transfer efficiency is not 100 %.

We are interested in the modeling, simulation and analysis of 2D/3D active integrated optical microresonator devices. The present work is embedded in the frame work of the European Commission funded research project NAIS (*"Next generation Active Integrated optical Subsystems"*). Check `http://www.mesaplus.utwente.nl/nais/` for details.

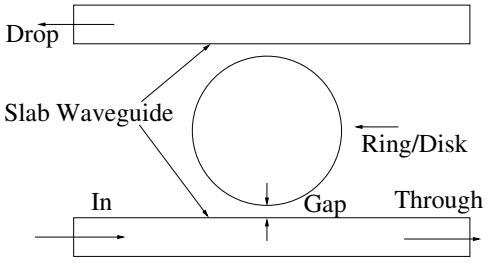

Figure 1.1: Schematic Microresonator

In this thesis, we report the spatial couple mode theory based modeling of microresonator. A symmetric dual coupling microresonator device is functionally decomposed into two couplers each one consisting of a straight waveguide and a bent waveguide. These two couplers are internally connected to each other

by two other bent waveguides. Each coupler is externally connected to two other straight waveguides. The advantage of such decomposition is that the modeling of a microresonator reduces to the modeling of a bent waveguide and the modeling of the coupler involving a bent waveguide and a straight waveguide.

1.2 Outline of Thesis

Our main interest is the modeling of microresonator. In section 1.3 we give the literature review of different techniques used for such modeling. For the version of the spatial couple mode theory in which we are interested, we need modes of the bent waveguide. In chapter 2 we present the modeling of the bent waveguide. Using this model, a semi analytical bend mode solver is implemented. The simulation results of this bend mode solver are discussed in chapter 3. In chapter 4 we present the spatial couple mode theory based model of a coupler involving a bent waveguide and a straight waveguide. In chapter 5, we discuss the modeling of microresonator in terms of coupler involving a bent waveguide. By knowing the so called scattering matrix of the coupler, we can completely characterise the microresonator. Complementary important results are provided in the appendixes.

1.3 The Literature Review

Here we present an overview of the state of the art modeling and simulation techniques for MRs. Our specific interest is *coupled mode* based modeling of MRs. We also pay attention to the use of anisotropic material for MRs and their application as filters. The references are broadly classified as follows:

- As either a *'Experimental'* work or as a *'Theoretical'* work.
- When just an isolated cavity (microdisk/microring/microsphere) is considered, it is classified as the *'Cavity'*. When it is coupled to a straight waveguide with application as a frequency selector, it is classified as a *'Filter'*.
- A *Frequency domain approach* in which filter operation is analysed in terms of light frequency as a given parameter, as in the scattering matrix method, conformal mapping method or coupling of modes in space method. A *time domain approach* like a coupling of modes in time method, finite difference time domain methods.

	Experimental	Theoretical
Cavity	[4], [20], [56]	[17], [41], [13], [47], [28]
Filter	[4], [7], [8], [23], [29], [31], [32], [34] [2], [3], [10], [15], [51],[16], [19], [34]	[8], [14], [18], [31], [39], [48], [52], [54] [22], [24], [38], [37], [40], [43]

- **General:** A good introduction to the working of MR and different coupling types is given in [32]. High finesse cylindrical MR can be realized with either laterally or vertically straight waveguide (SW) coupling. This paper concludes that even though laterally SW coupled MRs can be realized by simple (e.g. single mask) processes), they are less versatile and more sensitive to technological variations than vertically SW coupled MRs. Arguing on the basis of the propagation loss, in [51] the authors also come to the same conclusion.
- **Scattering matrix approach:** Intuitive scattering matrix method is used to model MRs [46, 49]. In [54] using a scattering matrix method, generic relations for coupling of optical power between microring and single/double dielectric waveguides are derived. The author shows that for the *critical coupling* of a single waveguide with a microcavity, the internal losses should be equal to the coupling losses. The presence of a second waveguide modifies the internal loss parameter. For full power transfer from the input waveguide to the output waveguide, this leads to conditions that internal losses should be negligible and two waveguide to microring couplers should be identical. Thus by controlling this coupling, power transfer can be controlled in MR. This theory was tested experimentally in [15, 16].

- **Method of conformal mapping:** Conformal mapping is one of the frequently used method for analyzing MR. In [13], a conformal mapping method is used to find out modal fields in 'microdisk'. This approach is motivated by the use of conformal mapping for finding modes of bent waveguides. This approach was extended to MRs in [14], where a MR is analyzed by using the conformal mapping along with the effective index method (EIM). This analysis is used to compute coupling coefficient, losses and Q of a MR.
  In [17], conformal mapping is used to analyse a concentric microcavities device as a laser source.

- **Coupled mode theory:** Due to its conceptual simplicity and physical insight, Coupled Mode Theory (CMT) is the most widely used method for analyzing MRs. The coupling of modes can be formulated either in space or in time.

  A general theoretical discussion of space dependent CMT is presented in [46, chapter 4]. [48] gives a coupled mode formulation based on coupling of modes in space for MRs. This approach is also known as the *directional coupler approach* [21]. Using CMT in combination with scattering matrix formulation, the operation of MR can be described in terms of a *coupling coefficient* and a *propagation constant*.

  In [29], the authors argue that above approach may not be useful for extremely small MRs. The resonance of an uncoupled resonator can be characterized by either the propagation constant or the frequency, which are related to each other by a *dispersion relation*. But when a resonator is coupled to a waveguide, both play different roles. In this paper, it's author elaborates the difference in choosing either the propagation constant or the frequency as a parameter for small MRs. This fact is exploited to excite a broad range of resonance modes by controlling the size of the resonator.

  In a MR, in a resonance state the rate of the energy decay is related to the coupling coefficient. A time dependent CMT [38, 43] is based on this correspondence between the circulating power and the ring energy. The general theoretical discussion for a time dependent CMT is presented in [27, chapter 7]. The advantage of a time dependent CMT is that the coupled mode equations are simpler than that of a space based formulation. In [18], a time dependent CMT is used to analyze the operation and design of a active semiconductor MR, specially to understand the design trends and constraints for MR.

- **Other analytical methods:** [22] discuss analytical methods like spectral index method, full wave integral equation, analytical regularization etc. In [47, 28] a microring/microdisk is analysed by method of moments.

- **Numerical methods:** Use of numerical methods is motivated by its success in analyzing microwave devices and solving the bend mode problem in optical regime. In [35] using Rayleigh-Ritz and the finite element method analysis of WGM in anisotropic dielectric resonators (in the microwave regime) is carried out. The authors claim accurate estimation of losses with this method. [24] discusses the finite difference time domain (FDTD) approach for MRs, [37] discusses FDTD method for computation of WGMs. In [33], intensity profiles of the WGMs are computed using EIM and finite difference methods for bends as in [42].

- **Experimental:** In [23], experimental results for single mode, single microring GaInAsP-InP optical channel dropping filter are discussed. The authors also discuss material and realization issues. Non linear optical material with intensity dependent refractive index can be used for MR realization [8, 52]. In [8], a scattering matrix method (also known as a transfer matrix method) is used to analyse the device. In this work, the author faces several difficulties in achieving high Q which he attributes to the misalignment between the SW and the microring and the occurrence of high order radial WGMs.

  [2] discusses the realization and experimental results of vertically coupled MRs using polymer wafer bonding. A polarization independent vertically coupled microring resonator filter using a birefringent polymer overlay is proposed in [34].

[19] investigates the dependence of the quality factor and the power extraction coefficient on various structural parameters of MR. e.g. disk radius, coupling separation, straight waveguide dimensions.

In [7] a two mask based new MR design is proposed, which allows better refractive index contrast optimization for the SW and the MR. i.e. low index contrast for the SW for better fiber-to-chip coupling and high index contrast for resonator for low bend loss. Realization and experimental output of the proposed design is discussed.

- **Use of the Microscope:** Unlike conventional microscopy, in Photon Scanning Tunneling Microscopy (PSTM) the spatial resolution is determined by the size of the aperture of the optical fiber tip rather than by the wavelength of the light used. This property is used to map the optical field inside the MR using PSTM [4, 3]. This information is used to study the intercavity phenomena like polarization conversion, interference of co-propagating and contra-propagating modes. The theoretical framework for this work is developed in [31]. In this paper, a parametric model based on only real angular propagation constant and Free Spectral Range (FSR) of the intercavity intensity is presented. Based on this model, the wavelength and spatial dependence of the intercavity intensity is described.

  Like PSTM, Total Internal Reflection Microscopy is used to map inter-cavity fields [29].

- **Addressing polarization issue:** Though MRs are versatile in several aspects, before employing it for dense integration, several issues like the high propagation loss, polarization dependent behavior etc. has to be addressed.
  For polarization independent operation, both TE and TM modes must resonate at the same wavelength. One way to achieve this is to adjust the aspect ratio of a ring structure, but maintaining the single mode operation in both polarizations. It can be achieved by using strong form birefringence of the high index bend waveguide that constitute the cavity. In [34], authors propose an overlay of birefringent polymer to compensate for the large form birefringence of the MR and demonstrate the polarization independent operation.

- **Addressing losses in MRs:** For a realistic modeling of a MR as a filter, it is important to study the effect of the radiation and the absorption losses on the performance of the filter. The quality of a resonator (Q) is affected by a radiation loss.

  [7] discusses the realization and experimental results of vertically coupled MR using polymers and suggests improvements for reducing the radiation loss in MR. [9] discusses numerically exact analysis and modeling results for radiation and absorption losses of 2D cylindrical MRs (in the microwave regime). The authors use the *method of analytical regularization* for it. They claim that it provides guaranteed convergence and controlled accuracy of computations even at the sharp resonances, unlike the conventional method of moments and finite element techniques.

  In [51], it is shown that the round trip propagation loss in a small radius racetrack MRs can be minimized by introducing a lateral offset at the straight-to-bend waveguide junctions.

- **Addressing coupling issue:** Apart from integrated optical waveguides, light is coupled to microring by evanescent coupling employing prism coupler, tapered fiber or polished half block coupler. The analytic theory of coupling from tapered fibers and half blocks into 'microsphere' resonators is developed in [40].

  [10] reports that low intrinsic cavity loss and a symmetric dual coupling structure are crucial for obtaining high coupling efficiency. In unsymmetric coupling the intrinsic loss was observed to be nearly independent of the mode index of the WGM. But in a dual coupling case, the output coupler introduces a mode dependent loss to the resonant modes that influences the coupling through the first coupler. Thus *the symmetrical dual coupling structure maintains a critical coupling condition for a wide range of modes.* With this technique, authors in this paper demonstrate 99% power transfer to WGM in MRs. The possibility of using electro-optic effects for controlling the critical coupling is discussed in [55].

Chapter 2

Modeling of Bent Waveguide

In Photonic Integrated Circuits (PICs), bent waveguides play very important role. They are used to connect input-output ports of different devices. Alternatively T-junctions with deep etched mirrors (as bifurcators) or corner bends with mirrors were employed as bends. In case of deep etched mirrors, a small dislocation or a tilt of a mirror increases the loss. Also mirrors can not be used in buried waveguide structures [30]. Bent waveguides do not suffer from such problems and technically feasible to incorporate them in buried structures. On the other hand, there are losses due to bending of waveguide. *Thus from a design point of view, an accurate estimation of a attenuation constant (α) and a phase constant (β) for bent waveguides is very important.*

The cost of photonic devices can be reduced by integrating various components on a wafer and then by mass production. In this sense, it is advantageous to minimize the bend radius as much as possible without introducing significant loss and optimize the use of wafer area for higher packing density of components.

But when an optical waveguide is bent, radiation loss occurs. This can be explained physically by the bounded speed of the electromagnetic waves [5, pp. 31]. Due to boundedness of speed of the electromagnetic wave, straight wave fronts in a curved waveguide can not occur. The curvature of the wave front gives rise to radiation away from the waveguide, as shown in fig. 2.1. This makes modal the propagation constant (γ) essentially complex valued, where the non vanishing imaginary part of γ corresponds to the radiation effect due to the bend.

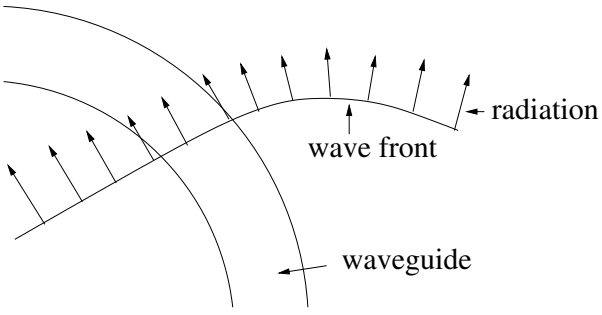

Figure 2.1: Radiation in curved waveguide

It is found that as the bend radius decreases, the modal field shifts towards the outer core/cladding interface. Also as the radius decreases, the attenuation constant increases. The thorough understanding of effects of waveguide geometry and index profiles on bending loss is necessary for efficient and reliable design of bends in PICs.

2.1 Model Description

Consider the bent slab waveguide structure with the y axis as the axis of symmetry as shown in fig.2.2. We assume that the material properties and the field do not vary in the y direction. We use the cylindrical co-ordinate system (r, y, θ) as a reference co-ordinate system. In this system, let the functional form of the propagating electric field ($\mathbf{E}$) and the magnetic field ($\mathbf{H}$) be as

$$\mathbf{E}(r, y, \theta, t) = (E_r(r), E_y(r), E_\theta(r)) = (E_r^0(r), E_y^0(r), E_\theta^0(r))e^{i(\omega t - \gamma R\theta)} \quad (2.1)$$

$$\mathbf{H}(r, \theta, y, t) = (H_r(r), H_y(r), H_\theta(r)) = (H_r^0(r), H_y^0(r), H_\theta^0(r))e^{i(\omega t - \gamma R\theta)} \quad (2.2)$$

where $E_r(r), E_y(r), E_\theta(r)$ represent r, y and θ the components of modal electric field of resp., E_r^0, E_y^0 and E_θ^0 represent corresponding mode profiles. Similar notations holds for the magnetic field. γ is the *propagation constant* of the bend mode. The physical electric and magnetic field is the real part of $\mathbf{E}$ and $\mathbf{H}$ resp. Since an electromagnetic field propagating through a bent loses energy due to radiation, γ is complex valued, denote $\gamma = \beta - i\alpha$, where β is the *phase constant* which is a measure of the phase velocity of a propagating wave and α is the *attenuation constant* which is a measure of the radiation loss.

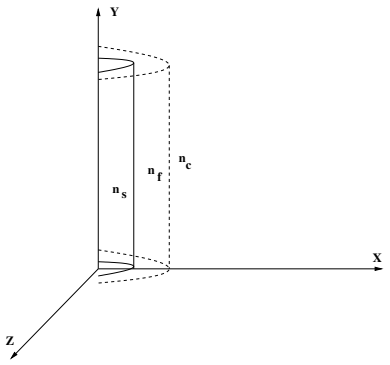

Figure 2.2: 3 D bent waveguide

Consider the (x, z) or (r, θ) plane as shown in fig.2.3. n_c, n_f and n_s are the cladding, film and substrate refractive indices resp. Let R be the bent radius and d be the bent width.

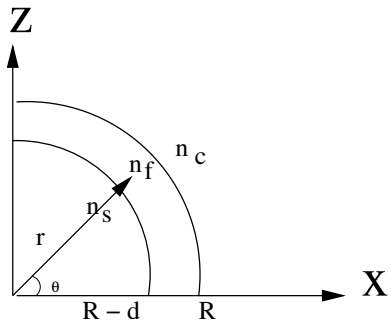

Figure 2.3: 2 D Bent waveguide

We take the outer layer interface as radius R and inner layer interface as $R - d$. Other choices are possible, like in [53], take outer layer interface as $R + d/2$ and inner layer interface as $R - d/2$.

2.2 Component Dependency

Here we will find out the component dependency in our model problem. Using the definition of $\mathbf{E}$ and $\mathbf{H}$ as in (2.1) and (2.2) resp., we have

$$\begin{aligned}\nabla \times \mathbf{E} &= \frac{1}{r}\begin{vmatrix} a_r & a_y & ra_\theta \\ \frac{d}{dr} & 0 & \frac{d}{d\theta} \\ E_r^0 e^{i(\omega t-\gamma R\theta)} & E_y^0 e^{i(\omega t-\gamma R\theta)} & rE_\theta^0 e^{i(\omega t-\gamma R\theta)} \end{vmatrix} \\ &= \frac{1}{r}\left[a_r\left(i\gamma R E_y^0\right) - a_y\left(\frac{drE_\theta^0}{dr} + i\gamma R E_r^0\right) + ra_\theta\left(\frac{dE_y^0}{dr}\right)\right]\cdot e^{i(\omega t-\gamma R\theta)}\end{aligned}$$

Using the relation

$$\nabla \times \mathbf{E} = -i\mu_0\omega\mathbf{H}$$

we get

$$\frac{\gamma R}{r}E_y^0 = -\mu_0\omega H_r^0 \tag{2.3}$$

$$\frac{dE_y^0}{dr} = -i\mu_0\omega H_\theta^0 \tag{2.4}$$

$$\frac{1}{r}\frac{drE_\theta^0}{dr} + \frac{i\gamma R}{r}E_r^0 = i\mu_0\omega H_y^0 \tag{2.5}$$

$$\frac{\gamma R}{r}H_y^0 = \epsilon_0\epsilon\omega E_r^0 \tag{2.6}$$

$$\frac{dH_y^0}{dr} = i\epsilon_0\epsilon\omega E_\theta^0 \tag{2.7}$$

$$-\frac{1}{r}\frac{drH_\theta^0}{dr} - \frac{i\gamma R}{r}H_r^0 = i\epsilon_0\epsilon\omega E_y^0 \tag{2.8}$$

Classification of modes

Analyzing eq.(2.3) to eq.(2.8) we see that, above set of eq.s can be grouped as two decoupled sets as (eq.(2.3), eq.(2.4), eq.(2.8)) and (eq.(2.5), eq.(2.6), eq.(2.7)).

- **Transverse Electric waves (TE)** : For TE wave, there is no component of electric field in the direction of propagation. i.e $E_r^0 = 0 = E_\theta^0$ and so $H_y^0 = 0$. Note that $E_y^0 \neq 0$ and knowing E_y^0, we can solve for TE wave i.e. E_y^0, H_r^0, H_θ^0.
- **Transverse Magnetic waves (TM)** : For TM wave, there is no component of magnetic field in the direction of propagation. i.e $H_r^0 = 0 = H_\theta^0$ and so $E_y^0 = 0$. Note that $H_y^0 \neq 0$ and knowing H_y^0, we can solve for TM wave i.e. H_y^0, E_r^0, E_θ^0.

Thus it is enough to know E_y^0 and H_y^0, to determine completely the electromagnetic field distribution for a given model.

2.3 Energy Flow Density

The power density associated with a TE bend mode is given by the time average Poynting vector $\mathbf{S_{av}}$.

$$\begin{aligned}
\mathbf{S}_{\text{av}} &= \frac{1}{2}\Re(\mathbf{E}\times\mathbf{H}^*) \\
&= \frac{1}{2}\Re\begin{vmatrix} \mathbf{a}_r & \mathbf{a}_y & \mathbf{a}_\theta \\ E_r & E_y & E_\theta \\ H_r^* & H_y^* & H_\theta^* \end{vmatrix} \\
&= \frac{1}{2}\Re\begin{vmatrix} \mathbf{a}_r & \mathbf{a}_y & \mathbf{a}_\theta \\ 0 & E_y & 0 \\ H_r^* & 0 & H_\theta^* \end{vmatrix} \\
&= \frac{1}{2}\Re(\mathbf{a}_r(H_\theta^*\cdot E_y) - \mathbf{a}_\theta(H_r^*\cdot E_y)) \\
&= \frac{1}{2}\Re(\mathbf{a}_r(H_\theta^{0^*}E_y^0 e^{-2\alpha R\theta}) - \mathbf{a}_\theta(H_r^{0*}\cdot E_y^0 e^{-2\alpha R\theta}))
\end{aligned}$$

Using eq. (2.3) and (2.4)

$$H_\theta^0 = \frac{i}{\mu_0\omega}\frac{\partial E_y^0}{\partial r} \qquad H_r^0 = -\frac{\gamma R}{r}\frac{1}{\mu_0\omega}E_y^0$$

$$\mathbf{P}_{\text{av}} = \frac{1}{2}\Re\left[\mathbf{a}_r\left[-\frac{i}{\mu_0\omega}\frac{\partial E_y^{0^*}}{\partial r}E_y^0 e^{-2\alpha R\theta}\right] + \mathbf{a}_\theta\left[\frac{\gamma^* R}{r}\frac{1}{\mu_0\omega}|E_y^0|^2 e^{-2\alpha R\theta}\right]\right]$$

$$\text{The power flow in radial direction} = P_{av,r} = -\frac{e^{-2\alpha R\theta}}{2\mu_0\omega}\Re\left[iE_y^0\frac{\partial E_y^{0^*}}{\partial r}\right] \tag{2.9}$$

$$\text{The power flow in angular direction} = P_{av,\theta} = \frac{R}{r}e^{-2\alpha R\theta}\frac{\beta}{2\mu_0\omega}|E_y^0|^2 \tag{2.10}$$

The total power transported in the angular direction ($\int P_{av,\theta}\, dr$) is called as *modal power*.[1]

2.4 Solving for E_y^0

Consider the set of equations {(2.3), (2.4), (2.8)}. Put the value of H_r^0 from eq.(2.3) and the value of H_θ^0 from eq.(2.4) into eq.(2.8). This leads to

$$r^2\frac{d^2E_y^0}{dr^2} + r\frac{dE_y^0}{dr} + (n^2k_0^2r^2 - \gamma^2R^2)E_y^0 = 0 \tag{2.11}$$

This is the governing eq. for E_y^0, which is a *Bessel equation* with complex order γR. Here $n = n(r)$ is the refractive index of the medium (in our model problem, it is piecewise constant), $k_0 = \frac{2\pi}{\lambda}$ is the wavenumber in free space corresponding to a given vacuum wavelength (λ).

Let $E_{y,s}^0, E_{y,f}^0, E_{y,c}^0$ be the y component of electric field in substrate, film and cladding medium resp.

[1] For a straight waveguide, the total modal power is given by

$$P_{\text{modal}} = \frac{\beta}{2\mu_0\omega}\int |E_y^0|^2\, dx$$

- In the substrate, the general solution for electric field is a linear combination of the Bessel function of the first kind (J) and the Bessel function of the second kind (Y) as

$$E_{y,s}^0 = C_s J_{\gamma R}(n_s k_0 r) + D_s Y_{\gamma R}(n_s k_0 r)$$

  There is no source or sink in the substrate region. As $r \longrightarrow 0$, the Bessel function of second kind (Y) tends to $-\infty$. For the boundedness of electric field in the substrate region, $D_s \equiv 0$.

$$E_{y,s}^0 = C_s J_{\gamma R}(n_s k_0 r) \tag{2.12}$$

- In the film, the general solution for the electric field will be as

$$E_{y,f}^0 = C_f J_{\gamma R}(n_f k_0 r) + D_f Y_{\gamma R}(n_f k_0 r) \tag{2.13}$$

- In the cladding, we are looking for decaying solution. We can represent such solution for the electric field either in terms of the Hankel function of the first kind ($H^{(1)}$) or in terms of the Hankel function of the second kind ($H^{(2)}$). (See the asymptotic expansion for Hankel functions. These are decaying as square root of r.)

  Case I:
  In the cover region, let

$$E_y^0 = D H_\nu^{(1)}(n_c k_0 r)$$

  where D is an unknown constant. For $r \to \infty$, using the asymptotic expansion for Hankel function of first kind given by (B.1), it can be shown that the power flow in the radial direction is given by

$$P_{\text{av,r}} = -\frac{|D|^2}{\mu_0 \omega} \frac{1}{\pi r} e^{\alpha R(\pi - 2\theta)}$$

  With the choice of $H^{(1)}$, for large r, power is flowing towards waveguide and therefore $H^{(1)}$ represents incoming wave. Note that, multiplying asymptotic expansion by time harmonic $\exp(i\omega t)$, it is clear that $H_\nu^{(1)}$ represents incoming wave.

  Case II:
  In cover region, let

$$E_y^0 = D H_\nu^{(2)}(n_c k_0 r)$$

  where D is an unknown constant. For $r \to \infty$, using the asymptotic expansion for Hankel function of second kind given by (B.2), it can be shown that the power flow in the radial direction is given by

$$P_{\text{av,r}} = \frac{|D|^2}{\mu_0 \omega} \frac{1}{\pi r} e^{\alpha R(\pi - 2\theta)}$$

  With the choice of $H^{(2)}$, for large r, power is flowing away from waveguide and therefore $H^{(2)}$ represents outgoing wave. Note that, multiplying asymptotic expansion by time harmonic $\exp(i\omega t)$, it is clear that $H_\nu^{(2)}$ represents outgoing wave.

  Only $H^{(2)}$ representes outgoing and decaying wave for $r \to \infty$, therefore

$$E_{y,c}^0 = D_c H_{\gamma R}^{(2)}(n_c k_0 r) \tag{2.14}$$

Thus the piecewise defined ansatz for the bend mode profile is

$$E_y^0(r) = \begin{cases} E_{y,s}^0 = C_s J_{\gamma R}(n_s k_0 r) & 0 \le r \le R - d \\ E_{y,f}^0 = C_f J_{\gamma R}(n_f k_0 r) + D_f Y_{\gamma R}(n_f k_0 r) & R - d \le r \le R \\ E_{y,c}^0 = D_c H_{\gamma R}^{(2)}(n_c k_0 r) & r \ge R \end{cases} \tag{2.15}$$

The following interface conditions has to be satisfied by $E_y^0(r)$

- The tangential component of **E** is continuous across the interface i.e. E_y^0 is continuous across the interface.

$$E_{y,s}^0(R-d) = E_{y,f}^0(R-d)$$
$$C_s J_{\gamma R}(n_s k_0(R-d)) = C_f J_{\gamma R}(n_f k_0(R-d)) + D_f Y_{\gamma R}(n_f k_0(R-d)) \tag{2.16}$$
$$E_{y,f}^0(R) = E_{y,c}^0(R)$$
$$C_f J_{\gamma R}(n_f k_0 R) + D_f Y_{\gamma R}(n_f k_0 R) = D_c H_{\gamma R}^{(2)}(n_c k_0 R) \tag{2.17}$$

- The tangential component of **H** is continuous across the interface i.e. H_θ^0 is continuous across the interface. From eq.(2.4), this is equivalent to continuity of $\frac{dE_y^0}{dr}$ across the interface.

$$\left.\frac{dE_{y,s}^0}{dr}\right|_{r=R-d} = \left.\frac{dE_{y,f}^0}{dr}\right|_{r=R-d}$$
$$C_s n_s k_0 J_{\gamma R}^{'}(n_s k_0(R-d)) = C_f n_f k_0 J_{\gamma R}^{'}(n_f k_0(R-d)) + D_f n_f k_0 Y_{\gamma R}^{'}(n_f k_0(R-d)) \tag{2.18}$$
$$\left.\frac{dE_{y,f}^0}{dr}\right|_{r=R} = \left.\frac{dE_{y,c}^0}{dr}\right|_{r=R}$$
$$C_f n_f k_0 J_{\gamma R}^{'}(n_f k_0 R) + D_f n_f k_0 Y_{\gamma R}^{'}(n_f k_0 R) = D_c n_c k_0 H_{\gamma R}^{(2)'}(n_c k_0 R) \tag{2.19}$$

In matrix form $Ax = 0$, the above eq.s can be written as

$$\begin{bmatrix} J_\nu(n_s k_0 R^-) & -J_\nu(n_f k_0 R^-) & -Y_\nu(n_f k_0 R^-) & 0 \\ 0 & J_\nu(n_f k_0 R^+) & Y_\nu(n_f k_0 R^+) & -H_\nu^{(2)}(n_c k_0 R^+) \\ n_s J_\nu^{'}(n_s k_0 R^-) & -n_f J_\nu^{'}(n_f k_0 R^-) & -n_f Y_\nu^{'}(n_f k_0 R^-) & 0 \\ 0 & n_f J_\nu^{'}(n_f k_0 R^+) & n_f Y_\nu^{'}(n_f k_0 R^+) & -n_c H_\nu^{(2)'}(n_c k_0 R^+) \end{bmatrix} \begin{bmatrix} C_s \\ C_f \\ D_f \\ D_c \end{bmatrix} = 0 \tag{2.20}$$

where

$$\nu = \gamma R \qquad R^- = R - d \qquad R^+ = R \tag{2.21}$$

A non trivial solution of above linear system of eq. exists iff $\det A = 0$. Therefore

$$|A| = \begin{vmatrix} J_\nu(n_s k_0 R^-) & -J_\nu(n_f k_0 R^-) & -Y_\nu(n_f k_0 R^-) & 0 \\ 0 & J_\nu(n_f k_0 R^+) & Y_\nu(n_f k_0 R^+) & -H_\nu^{(2)}(n_c k_0 R^+) \\ n_s J_\nu^{'}(n_s k_0 R^-) & -n_f J_\nu^{'}(n_f k_0 R^-) & -n_f Y_\nu^{'}(n_f k_0 R^-) & 0 \\ 0 & n_f J_\nu^{'}(n_f k_0 R^+) & n_f Y_\nu^{'}(n_f k_0 R^+) & -n_c H_\nu^{(2)'}(n_c k_0 R^+) \end{vmatrix} = 0$$

Let R_j is the j^{th} row, a_{jk} is j'th row and k'th column entry of matrix A. Using following row operations, the above equation can be simplified.

$$R_1 \longrightarrow \frac{R_1}{a_{11}}, R_3 \longrightarrow \frac{R_3}{a_{31}}, R_3 \longrightarrow R_3 - R_1$$
$$R_1 \longrightarrow \frac{R_1}{a_{13}}, R_3 \longrightarrow \frac{R_3}{a_{33}}, R_3 \longrightarrow R_3 - R_1$$

The above equation can be represented as follows:

$$\frac{\left[\frac{J_\nu(n_f k_0 R^-)}{J_\nu(n_s k_0 R^-)} - \frac{n_f}{n_s}\frac{J_\nu^{'}(n_f k_0 R^-)}{J_\nu^{'}(n_s k_0 R^-)}\right]}{\left[\frac{Y_\nu(n_f k_0 R^-)}{J_\nu(n_s k_0 R^-)} - \frac{n_f}{n_s}\frac{Y_\nu^{'}(n_f k_0 R^-)}{J_\nu^{'}(n_s k_0 R^-)}\right]} = \frac{\left[\frac{J_\nu(n_f k_0 R^+)}{H_\nu^{(2)}(n_c k_0 R^+)} - \frac{n_f}{n_c}\frac{J_\nu^{'}(n_f k_0 R^+)}{H_\nu^{(2)'}(n_c k_0 R^+)}\right]}{\left[\frac{Y_\nu(n_f k_0 R^+)}{H_\nu^{(2)}(n_c k_0 R^+)} - \frac{n_f}{n_c}\frac{Y_\nu^{'}(n_f k_0 R^+)}{H_\nu^{(2)'}(n_c k_0 R^+)}\right]} \tag{2.22}$$

This is a *dispersion equation* for TE modes of the bent slab waveguide. For a given frequency (ω), we solve this equation for the propagation constant (γ). Then we solve eq. (2.20) for the unknown coefficients which determine the mode profile (2.15).

Chapter 3

Bent Waveguide Mode Solver

In this chapter, we report the simulation results for the bent waveguide model that is described in the previous chapter. The semi analytic bent mode solver is implemented in Maple and in C++.

- The Maple version of bent mode solver is slow for large R. Therefore, it has been implemented in C++.
- The C++ bent mode solver was developed using the templet provided by author's supervisor Dr. Manfred Hammer. It was based up on straight waveguide mode solver developed by him.
- The C++ version of the bent mode solver uses complex order Bessel functions. Complex order Bessel functions routines were not available, therefore they are implemented. For details of its implementation, see appendix C.
- The dispersion equation 2.22 is solved using the secant method. The secant methods needs two complex initial guesses, which are formed by using β of equivalent straight waveguide as real part of initial guess with small imaginary part.

3.1 Simulations

The computations of above mode solvers are compared with that of from Vassallo [53, pp. 245]. The interface boundary definitions in this reference is different than ours. Note that the outer boundary in the setting of this literature is $R - d/2$.
Define a *loss factor* (n'') and *normalised effective permittivity* (B) as

$$n'' = \frac{\alpha}{k_0}, \qquad\qquad B = \frac{n_{eff}^2 - n_s^2}{n_f^2 - n_s^2}.$$

For structure with $(n_s, n_f, n_c) = (1.6, 1.7, 1.6)$, $d = 1\,\mu m$, $\lambda = 1.3\,\mu m$, the simulation results are as:

R [μm]	Vassallo's Results		Maple Results		C++ Results	
	n''	B	n''	B	n''	B
50	0.331e-3	0.6233	0.330932622e-3	0.6232872091	0.3309326e-03	0.6232872
100	0.266e-4	0.6024	0.198686814e-5	0.6023998242	0.1986868e-05	0.6023998
150	0.102e-7	0.5989	0.101947491e-7	0.5988742061	0.1019475e-07	0.5988742
200	0.508e-10	0.5977	0.506548821e-10	0.5976842758	0.5065440e-10	0.5976843

Table 3.1: Comparison I : For structure with $(n_s, n_f, n_c) = (1.6, 1.7, 1.6)$, $d = 1\,\mu m$, $\lambda = 1.3\,\mu m$

- Our Maple and C++ simulation results agree very well with the quoted results. Considering simulation time, C++ simulation was pretty fast compared to Maple.
- For $R = 100\,\mu m$, there is a difference in two results. As we show later on $\log_{10}(\alpha)$ varies linearly w.r.t. R. Vassallo's result don't show such behavior, while our result do satisfy it. We think it may be a *typo* in his book.

For this second numerical experiment, we took data from Vassallo[53, pp. 245].

R μm	Vasallos's Results		Maple Results		C++ Results	
	n''	B	n''	B	n''	B
200	0.642e-3	0.5977	0.2882074497e-3	0.5823226448	0.6427926e-3	0.5976695
400	0.254e-4	0.5627	0.2542728702e-4	0.5626675232	0.2542728e-4	0.5626675
600	0.884e-6	0.5555	0.8839801416e-6	0.5555285452	0.8839796e-6	0.5555285
800	0.289e-7	0.5532	0.2889781353e-7	0.5532198209	0.2889786e-7	0.5532198
1000	0.927e-9	0.5522	0.9257169823e-9	0.552190218	0.9256655e-9	0.5521902

Table 3.2: Comparison II: For structure with $(n_s, n_f, n_c) = (3.22, 3.26106.3.22)$, $d = 1\,\mu m$, $\lambda = 1.3\,\mu m$.

Field Profile

The field profile of E_y for settings in comparison I and for different radii is as shown in next figure. These plots clearly show the behavior of radiation in cover for increasing R. Observe the presence of strong radiation for small radius. These profiles were created by Dr. Manfred Hammer, check their animated version at `www.math.utwente.nl/~hammer/Nais/Bend/index.html`.

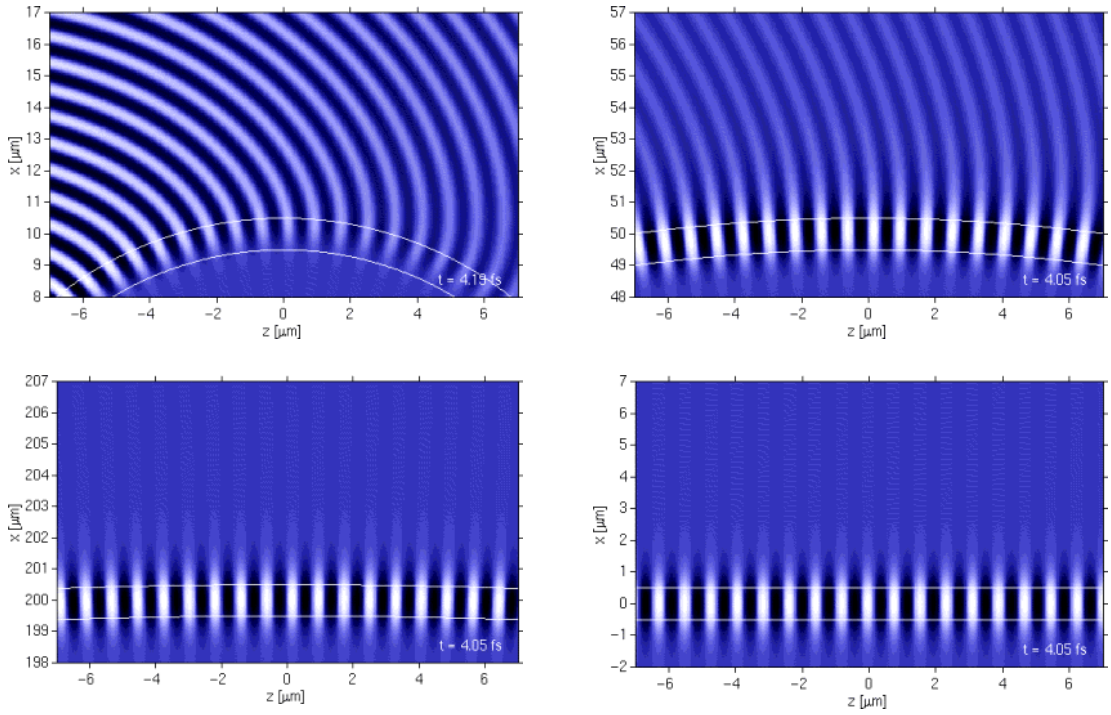

Figure 3.1: Animation clip shots for E_y for $(n_s, n_f, n_c) = (1.6, 1.7, 1.6)$, $d = 1\,\mu m$, $\lambda = 1.3\,\mu m$ with R equal to 10 μm, 50 μm, 100μm and ∞ (straight waveguide). White and black regions indicate positive and negative values, while grey color marks the zero level.

3.2 Analysing Bend Modes

To compare the field profiles for different radii, translate origin to R, scale the profile to a maximum absolute value of one and incorporate phase correction. Then the field profiles are as follows:

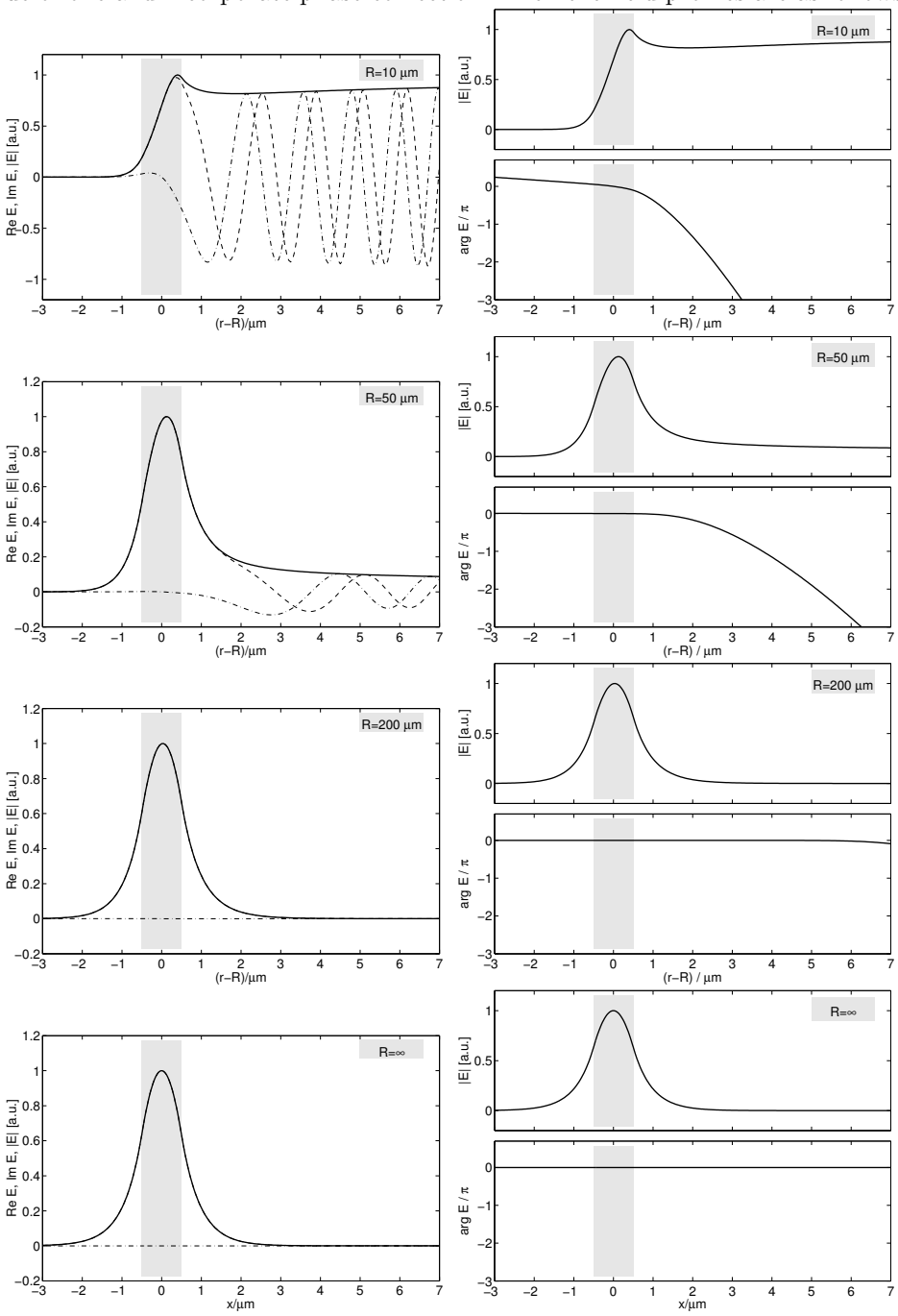

Figure 3.2: E_y Field profile for different radii for setting in comparison I. Plots on left hand side show absolute field (solid line), real part of field (dashed line) and the imaginary part of field (dash-dotted line). Plots on right hand side show absolute value and phase value for different radii. These plots are created by Dr. Manfred Hammer.

Observations

- Field is not well confined in core for smaller radius. But as R increases, confinement improves. For $R = 200\mu m$, field profile is similar to that of equivalent straight waveguide.
- The phase plot changes dramatically as R increases. For smaller R, phase curve is spherical in cover region, but as R increases, it tends to become a plane.

3.3 Variation of Propagation Constants with Bend Radius

Hence forth, all simulation results are obtained from C++ implementation. Here we analyse the effect of increasing radius on bent modes.

- The interfaces are at $R - d$ and R.
- The accuracy of the result depends upon the tolerance and maximum number of iterations allowed.

Consider the structure with $(n_s, n_f, n_c) = (1.6, 1.7, 1.6)$, $d = 1\,\mu m$, $\lambda = 1.3\,\mu m$. A few selected values of β and α for different radii are as:

$R\ [\mu m]$	$\alpha\ [\mu m^{-1}\ ]$	$\beta\ [\ \mu m^{-1}]$
10	1.254650e-01	7.771929e+00
50	1.663590e-03	7.957698e+00
100	1.006841e-05	7.987682e+00
150	5.177951e-08	7.999352e+00
200	2.575396e-10	8.005465e+00
250	1.260329e-12	8.009215e+00
∞	0	8.024803e+00

Table 3.3: Comparison I : For structure with $(n_s, n_f, n_c) = (1.6, 1.7, 1.6)$, $d = 1\,\mu m$, $\lambda = 1.3\,\mu m$. $R = \infty$ means corresponding straight waveguide.

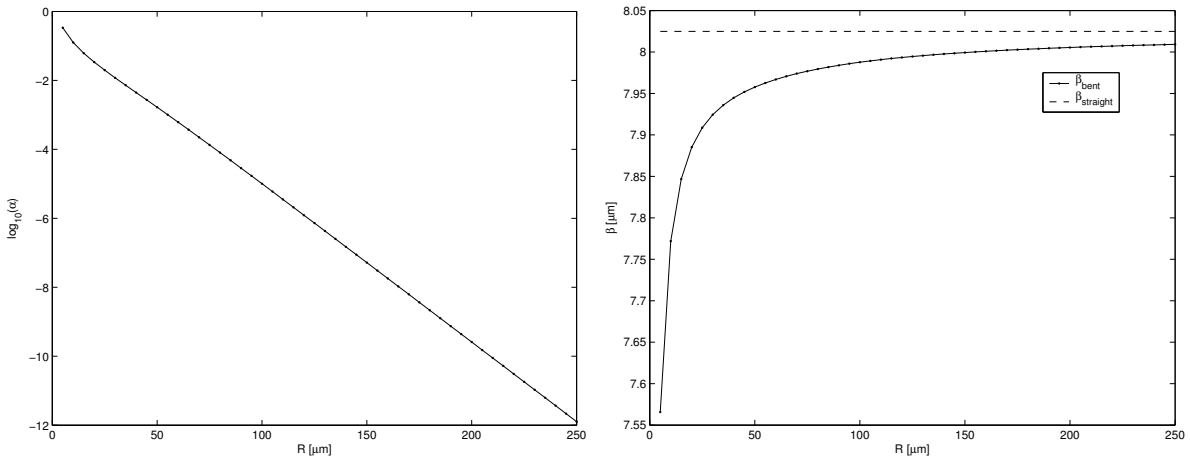

Figure 3.3: Variation of α and β against bent radius R for comparison I setting.

Observations

- It is found that *except for very small radius*, loss (α) decays exponentially w.r.t. R. i.e.

$$\alpha \propto e^{-c_1 R}$$

  where c_1 is a constant. For smaller radii, it seem dependence is not linear.

- As R increases, $\beta_{bend} \to \beta_{straight}$.

Consider the structure with $(n_s, n_f, n_c) = (3.22, 3.26106.3.22)$, $d = 1\,\mu m$, $\lambda = 1.3\,\mu m$. A few selected values of β and α for different radii are as:

$R\ [\mu m]$	$\alpha\ [\mu m^{-1}]$	$\beta\ [\mu m^{-1}]$
10	4.254161e-01	1.526186e+01
50	5.911844e-02	1.557242e+01
100	1.790224e-02	1.561931e+01
250	1.401331e-03	1.564750e+01
500	2.338092e-05	1.565834e+01
750	3.319726e-07	1.566270e+01
1000	4.510605e-09	1.566502e+01
∞	0	1.567251e+01

Table 3.4: Comparison II : For structure with $(n_s, n_f, n_c) = (3.22, 3.26106.3.22)$, $d = 1\,\mu m$, $\lambda = 1.3\,\mu m$. $R = \infty$ means corresponding straight waveguide.

Again we find the variation of β and α as in the previous case. Seethe next figure.

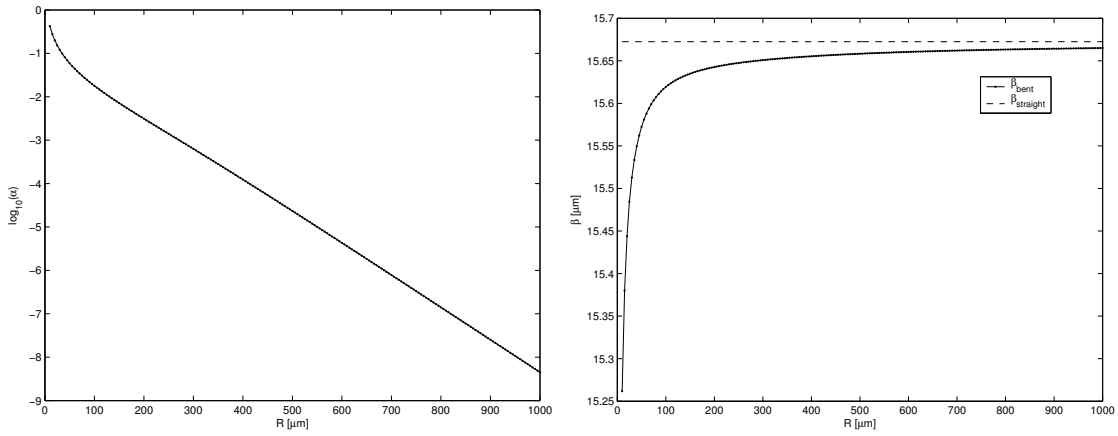

Figure 3.4: Variation of α and β against bent radius R for comparison II setting.

Chapter 4

Coupled Mode Theory

In this chapter, we describe a version of coupled mode theory for a coupler consisting of a bent waveguide and a straight waveguide. For the sake of brevity, we do not write the time dependence $e^{i\omega t}$ in following analysis. At appropriate places, time derivative is replaced by multiplication by factor $i\omega$. We use Cartesian co-ordinate system (x, y, z) as a reference system. We assume that the field and the material properties do not vary in the y direction. Later on for the sake of simplicity, we restrict our analysis to TE polarized fields.

4.1 General Theory

Let $\mathbf{E}_1$ and $\mathbf{H}_1$ be the electric and magnetic fields for the bent waveguide. $\mathbf{E}_1$ and $\mathbf{H}_1$ satisfy Maxwell eq.s

$$\nabla \times \mathbf{E}_1 = -i\mu_0\omega\mathbf{H}_1 \qquad\qquad \nabla \times \mathbf{H}_1 = i\epsilon_0\epsilon_1(x,z)\omega\mathbf{E}_1$$

where ϵ_1 gives relative permittivity distribution for bend structure.

Let $\mathbf{E}_2$ and $\mathbf{H}_2$ be the electric and magnetic fields for straight waveguide structure. $\mathbf{E}_2$ and $\mathbf{H}_2$ satisfy Maxwell eq.s

$$\nabla \times \mathbf{E_2} = -i\mu_0\omega\mathbf{H_2} \qquad\qquad \nabla \times \mathbf{H_2} = i\epsilon_0\epsilon_2(x,z)\omega\mathbf{E_2}$$

where ϵ_2 gives relative permittivity distribution for straight waveguide.

For the coupled structure, let the electric field $\mathbf{E}$ and magnetic field $\mathbf{H}$ be as following:

$$\mathbf{E}(x,z) = A(z)\mathbf{E}_1(x,z) + B(z)\mathbf{E}_2(x,z) \tag{4.1}$$

$$\mathbf{H}(x,z) = A(z)\mathbf{H}_1(x,z) + B(z)\mathbf{H}_2(x,z) \tag{4.2}$$

where $A(z)$ and $B(z)$ are unknown amplitude coupling coefficients.
$\mathbf{E}$ and $\mathbf{H}$ should satisfy Maxwell eq.s

$$\nabla \times \mathbf{E} = -i\mu_0\omega\mathbf{H} \qquad\qquad \nabla \times \mathbf{H} = i\epsilon_0\epsilon(x,z)\omega\mathbf{E}$$

where ϵ gives relative permittivity distribution for the coupled structure.

Remark: Note that in the present setting $|A(z)|^2$ and $|B(z)|^2$ can not be directly interpreted as the power in the bent and the straight waveguide respectively. The total power in the z direction in the coupled structure is given by

$$P_z = \frac{1}{2}\Re\left[\int (\mathbf{E}\times\mathbf{H}^*)\cdot\mathbf{a}_z\, dx\right] \tag{4.3}$$

$$P_z = |A(z)|^2 \frac{1}{2}\Re\left[\int (\mathbf{E}_1 \times \mathbf{H}_1^*)\cdot \mathbf{a}_z \, dx\right] + |B(z)|^2 \frac{1}{2}\Re\left[\int (\mathbf{E}_2 \times \mathbf{H}_2^*)\cdot \mathbf{a}_z \, dx\right] \quad (4.4)$$

$$+A(z)^* B(z)\Re\int (\mathbf{E}_2 \times \mathbf{H}_1^*)\cdot \mathbf{a}_z \, dx + A(z)B(z)^*\Re\int \mathbf{E}_1 \times \mathbf{H}_2^* \cdot \mathbf{a}_z \, dx \quad (4.5)$$

If the bent and straight waveguides modes are normalised (in Cartesian coordinate system) to a unit power, then

$$P_z = |A(z)|^2 + |B(z)|^2 + \Delta P$$

where

$$\Delta P = A(z)^* B(z)\Re\int (\mathbf{E}_2 \times \mathbf{H}_1^*)\cdot \mathbf{a}_z \, dx + A(z)B(z)^*\Re\int \mathbf{E}_1 \times \mathbf{H}_2^* \cdot \mathbf{a}_z \, dx$$

The term ΔP is strictly zero only when the coupled modes are two modes of the same unperturbed waveguide, which are coupled by perturbation of that waveguide. For lossless and weak coupling, i.e. when two lossless individual waveguides are sufficiently apart, it can be neglected. But in the present case, due to bending losses, ΔP can not be neglected. So we can not interprete $|A(z)|^2 + |B(z)|^2$ as power in the coupled structure.

Lorentz Reciprocity Theorem

For any two electromagnetic fields given by $(\mathbf{E}_p, \mathbf{H}_p, \epsilon_0\epsilon_p)$ and $(\mathbf{E}_q, \mathbf{H}_q, \epsilon_0\epsilon_q)$, using Maxwell's equations, one can derive the following identity known as *Lorentz Reciprocity Theorem.*

$$\begin{aligned} \nabla\cdot(\mathbf{E}_p \times \mathbf{H}_q^* + \mathbf{E}_q^* \times \mathbf{H}_p) &= -i\omega\epsilon_0(\epsilon_p - \epsilon_q)\mathbf{E}_p \cdot \mathbf{E}_q^* \\ \int \nabla\cdot(\mathbf{E}_p \times \mathbf{H}_q^* + \mathbf{E}_q^* \times \mathbf{H}_p)\, dx &= -i\omega\epsilon_0 \int (\epsilon_p - \epsilon_q)\mathbf{E}_p \cdot \mathbf{E}_q^* \, dx \end{aligned} \quad (4.6)$$

For $(\mathbf{E}, \mathbf{H}, \epsilon_0\epsilon)$ and $(\mathbf{E}_1, \mathbf{H}_1, \epsilon_0\epsilon_1)$, the Lorentz reciprocity relationship given by eq. (4.6) becomes

$$\int \nabla\cdot(\mathbf{E} \times \mathbf{H}_1^* + \mathbf{E}_1^* \times \mathbf{H})dx = -i\omega\epsilon_0 \int (\epsilon - \epsilon_1)\mathbf{E}\cdot\mathbf{E}_1^* \, dx$$

For $(\mathbf{E}, \mathbf{H}, \epsilon_0\epsilon)$ and $(\mathbf{E}_2, \mathbf{H}_2, \epsilon_0\epsilon_2)$, Lorentz reciprocity relationship given by eq. (4.6) becomes

$$\int \nabla\cdot(\mathbf{E} \times \mathbf{H}_2^* + \mathbf{E}_2^* \times \mathbf{H})dx = -i\omega\epsilon_0 \int (\epsilon - \epsilon_2)\mathbf{E}\cdot\mathbf{E}_2^* \, dx$$

Simplify above two equations using definitions of $\mathbf{E}$ and $\mathbf{H}$ given by eq. (4.1) and (4.2) and following vector identity

$$\nabla\cdot(\phi\mathbf{A}) = \phi\nabla\cdot\mathbf{A} + \mathbf{A}\cdot\nabla\phi$$

and we get

$$\begin{aligned} &\begin{bmatrix} \int \mathbf{a}_z\cdot(\mathbf{E}_1 \times \mathbf{H}_1^* + \mathbf{E}_1^* \times \mathbf{H}_1)dx & \int \mathbf{a}_z\cdot(\mathbf{E}_2 \times \mathbf{H}_1^* + \mathbf{E}_1^* \times \mathbf{H}_2)dx \\ \int \mathbf{a}_z\cdot(\mathbf{E}_1 \times \mathbf{H}_2^* + \mathbf{E}_2^* \times \mathbf{H}_1)dx & \int \mathbf{a}_z\cdot(\mathbf{E}_2 \times \mathbf{H}_2^* + \mathbf{E}_2^* \times \mathbf{H}_2)dx \end{bmatrix} \begin{bmatrix} d_z A \\ d_z B \end{bmatrix} \\ &\qquad + \begin{bmatrix} \int \nabla\cdot(\mathbf{E}_1 \times \mathbf{H}_1^* + \mathbf{E}_1^* \times \mathbf{H}_1)dx & \int \nabla\cdot(\mathbf{E}_2 \times \mathbf{H}_1^* + \mathbf{E}_1^* \times \mathbf{H}_2)dx \\ \int \nabla\cdot(\mathbf{E}_1 \times \mathbf{H}_2^* + \mathbf{E}_2^* \times \mathbf{H}_1)dx & \int \nabla\cdot(\mathbf{E}_2 \times \mathbf{H}_2^* + \mathbf{E}_2^* \times \mathbf{H}_2)dx \end{bmatrix} \begin{bmatrix} A \\ B \end{bmatrix} \\ &\quad = -i\omega\epsilon_0 \begin{bmatrix} \int(\epsilon - \epsilon_1)\mathbf{E}_1\cdot\mathbf{E}_1^* dx & \int(\epsilon - \epsilon_1)\mathbf{E}_2\cdot\mathbf{E}_1^* dx \\ \int(\epsilon - \epsilon_2)\mathbf{E}_1\cdot\mathbf{E}_2^* dx & \int(\epsilon - \epsilon_2)\mathbf{E}_2\cdot\mathbf{E}_2^* dx \end{bmatrix} \begin{bmatrix} A \\ B \end{bmatrix} \end{aligned} \quad (4.7)$$

Again using Lorentz reciprocity theorem,

$$\begin{aligned}
\int \nabla \cdot (\mathbf{E}_1 \times \mathbf{H}_1^* + \mathbf{E}_1^* \times \mathbf{H}_1) dx &= 0 \\
\int \nabla \cdot (\mathbf{E}_2 \times \mathbf{H}_1^* + \mathbf{E}_1^* \times \mathbf{H}_2) dx &= -i\omega\epsilon_0 \int (\epsilon_2 - \epsilon_1)\mathbf{E}_2 \cdot \mathbf{E}_1^* dx \\
\int \nabla \cdot (\mathbf{E}_1 \times \mathbf{H}_2^* + \mathbf{E}_2^* \times \mathbf{H}_1) dx &= -i\omega\epsilon_0 \int (\epsilon_1 - \epsilon_2)\mathbf{E}_1 \cdot \mathbf{E}_2^* dx \\
\int \nabla \cdot (\mathbf{E}_2 \times \mathbf{H}_2^* + \mathbf{E}_2^* \times \mathbf{H}_2) dx &= 0
\end{aligned}$$

Then one obtains,

$$\begin{bmatrix} \int \mathbf{a}_z \cdot (\mathbf{E}_1 \times \mathbf{H}_1^* + \mathbf{E}_1^* \times \mathbf{H}_1) dx & \int \mathbf{a}_z \cdot (\mathbf{E}_2 \times \mathbf{H}_1^* + \mathbf{E}_1^* \times \mathbf{H}_2) dx \\ \int \mathbf{a}_z \cdot (\mathbf{E}_1 \times \mathbf{H}_2^* + \mathbf{E}_2^* \times \mathbf{H}_1) dx & \int \mathbf{a}_z \cdot (\mathbf{E}_2 \times \mathbf{H}_2^* + \mathbf{E}_2^* \times \mathbf{H}_2) dx \end{bmatrix} \begin{bmatrix} d_z A \\ d_z B \end{bmatrix}$$

$$= -i\omega\epsilon_0 \begin{bmatrix} \int (\epsilon - \epsilon_1)\mathbf{E}_1 \cdot \mathbf{E}_1^* dx & \int (\epsilon - \epsilon_2)\mathbf{E}_2 \cdot \mathbf{E}_1^* dx \\ \int (\epsilon - \epsilon_1)\mathbf{E}_1 \cdot \mathbf{E}_2^* dx & \int (\epsilon - \epsilon_2)\mathbf{E}_2 \cdot \mathbf{E}_2^* dx \end{bmatrix} \begin{bmatrix} A \\ B \end{bmatrix}. \tag{4.8}$$

4.2 Coupler Model

As a notation, we denote all the quantities concerned with the bent waveguide with subscript 1 and that of the straight waveguide by 2. The structure we are analysing is as following.

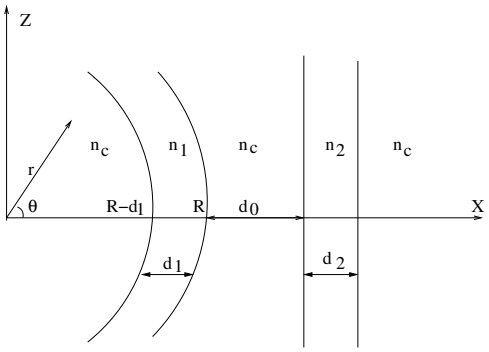

Figure 4.1: Part of 2D microresonator

Let n_c be the common background refractive index, n_1 is the core refractive index for the bent waveguide and n_2 is the core refractive index for the straight waveguide. Let d_1 and d_2 be the thickness of the bent and the straight waveguides resp. d_0 is the separation between them at $z = 0$ as shown in figure. R is the radius of bent waveguide.

Simplifications:

- Modeling in Cartesian co-ordinate system (x, y, z).
- No field variation in y direction.
- All individual structures are mono mode.
- TE polarised waves.
- Modes are forward propagating and there are no back reflections.

4.2.1 Bend Waveguide Fields

As described in section 2.1, 2.2, the bend mode field in cylindrical co-ordinate system (r, y, θ) with y axis as axis of symmetry is given by

$$\mathbf{E}_1(r,\theta,t) = (E_{1,r}, E_{1,y}, E_{1,\theta})(r,\theta)e^{i\omega t} = (E^0_{1,r}, E^0_{1,y}, E^0_{1,\theta})(r)e^{i(\omega t-\gamma_1 R\theta)} \quad (4.9)$$

$$\mathbf{H}_1(r,\theta,t) = (H_{1,r}, H_{1,y}, H_{1,\theta})(r,\theta)e^{i\omega t} = (H^0_{1,r}, H^0_{1,y}, H^0_{1,\theta})(r)e^{i(\omega t-\gamma_1 R\theta)} \quad (4.10)$$

$$E_{1,r}(r,\theta) = 0 \quad (4.11)$$

$$E_{1,y}(r,\theta) = E_{1,y}(r,\theta) = E^0_{1,y}(r)e^{-i\gamma_1 R\theta} \quad (4.12)$$

$$E_{1,\theta}(r,\theta) = 0 \quad (4.13)$$

$$H_{1,r}(r,\theta) = \frac{1}{r}\frac{-i}{\mu_0\omega}\partial_\theta E_{1,y}(r,\theta) = \frac{-1}{\mu_0\omega}\frac{\gamma_1 R}{r}E^0_{1,y}(r)e^{-i\gamma_1 R\theta} \quad (4.14)$$

$$H_{1,y}(r,\theta) = 0 \quad (4.15)$$

$$H_{1,\theta}(r,\theta) = \frac{i}{\mu_0\omega}\partial_r E_{1,y}(r,\theta) = \frac{i}{\mu_0\omega}\partial_r E^0_{1,y}(r)e^{-i\gamma_1 R\theta} \quad (4.16)$$

where $\gamma_1 = \beta_1 - i\alpha_1$ is a propagation constant and superscript zero denotes mode profile in respective directions.

Bend fields in Cartesian co-ordinate system

In final coupled mode analysis, we use Cartesian co-ordinate system. Therefore we transform above components from cylindrical to Cartesian co-ordinate system.

In our model, the y axis is the axis of symmetry for cylindrical co ordinate system. In such system, the relationship between the cylindrical components (A_r, A_y, A_θ) and the Cartesian components (A_x, A_y, A_z) is given by

$$\begin{bmatrix} A_x \\ A_y \\ A_z \end{bmatrix} = \begin{bmatrix} \cos\theta & 0 & -\sin\theta \\ 0 & 1 & 0 \\ \sin\theta & 0 & \cos\theta \end{bmatrix} \begin{bmatrix} A_r \\ A_y \\ A_\theta \end{bmatrix}$$

Therefore the components of a TE bend mode in the Cartesian system will be

$$\begin{aligned}
E_{1,x}(r(x,z),\theta(x,z)) &= 0 \\
E_{1,y}(r(x,z),\theta(x,z)) &= E_{1,y}(r,\theta) \\
E_{1,z}(r(x,z),\theta(x,z)) &= 0 \\
H_{1,x}(r(x,z),\theta(x,z)) &= \cos\theta\cdot\left[\frac{1}{r}\frac{-i}{\mu_0\omega}\partial_\theta E_{1,y}(r,\theta)\right] - \sin\theta\cdot\left[\frac{i}{\mu_0\omega}\partial_r E_{1,y}(r,\theta)\right] \\
H_{1,y}(r(x,z),\theta(x,z)) &= 0 \\
H_{1,z}(r(x,z),\theta(x,z)) &= \sin\theta\cdot\left[\frac{1}{r}\frac{-i}{\mu_0\omega}\partial_\theta E_{1,y}(r,\theta)\right] + \cos\theta\cdot\left[\frac{i}{\mu_0\omega}\partial_r E_{1,y}(r,\theta)\right]
\end{aligned}$$

Henceforth without loss of generality, above fields components are treated as a function of Cartesian co ordinates (x, z).

$$E_{1,x}(x,z) = 0 \quad (4.17)$$

$$E_{1,y}(x,z) = E^0_{1,y}(r)e^{-i\gamma_1 R\theta} \quad (4.18)$$

$$E_{1,z}(x,z) = 0 \quad (4.19)$$

$$H_{1,x}(x,z) = \frac{-i}{\mu_0\omega}\left[-\frac{i\gamma_1 R}{r}\cos\theta\ E^0_{1,y}(r) + \sin\theta\ \partial_r E^0_{1,y}(r)\right]e^{-i\gamma_1 R\theta} \quad (4.20)$$

$$H_{1,y}(x,z) = 0 \quad (4.21)$$

$$H_{1,z}(x,z) = \frac{-i}{\mu_0\omega}\left[-\frac{i\gamma_1 R}{r}\sin\theta\ E^0_{1,y}(r) - \cos\theta\ \partial_r E^0_{1,y}(r)\right]e^{-i\gamma_1 R\theta} \quad (4.22)$$

with $r = \sqrt{(x^2 + z^2)}$ and $\theta = \arctan z/x$.

4.2.2 Straight Waveguide Fields

The electromagnetic field in the straight waveguide is given by

$$\mathbf{E}_2(x,z,t) = (E_{2,x}, E_{2,y}, E_{2,z})(x,z)e^{i\omega t} = (E^0_{2,x}, E^0_{2,y}, E^0_{2,z})(x)e^{i(\omega t - \beta_2 z)} \quad (4.23)$$

$$\mathbf{H}_2(x,z,t) = (H_{2,x}, H_{2,y}, H_{2,z})(x,z)e^{i\omega t} = (H^0_{2,x}, H^0_{2,y}, H^0_{2,z})(x)e^{i(\omega t - \beta_2 z)} \quad (4.24)$$

$$E_{2,x}(x,z) = 0 \quad (4.25)$$

$$E_{2,y}(x,z) = E_{2,y}(x,z) = E^0_{2,y}(x)e^{-i\beta_2 z} \quad (4.26)$$

$$E_{2,z}(x,z) = 0 \quad (4.27)$$

$$H_{2,x}(x,z) = \frac{-i}{\mu_0\omega}\partial_z E_{2,y}(x,z) = \frac{-\beta_2}{\mu_0\omega}E^0_{2,y}(x)e^{-i\beta_2 z} \quad (4.28)$$

$$H_{2,y}(x,z) = 0 \quad (4.29)$$

$$H_{2,z}(x,z) = \frac{i}{\mu_0\omega}\partial_x E_{2,y}(x,z) = \frac{i}{\mu_0\omega}\partial_x E^0_{2,y}(x)e^{-i\beta_2 z} \quad (4.30)$$

where β_2 is the phase constant and superscript zero represents mode profile.

4.2.3 Coupled Mode Equations

For TE modes, CME (4.8), become

$$\begin{bmatrix} -\int(E^*_{1,y}H_{1,x} + E_{1,y}H^*_{1,x})\,dx & -\int(E^*_{1,y}H_{2,x} + E_{2,y}H^*_{1,x})\,dx \\ -\int(E_{1,y}H^*_{2,x} + E^*_{2,y}H_{1,x})\,dx & -\int(E_{2,y}H^*_{2,x} + E^*_{2,y}H_{2,x})\,dx \end{bmatrix} \begin{bmatrix} d_z A \\ d_z B \end{bmatrix} =$$

$$-i\omega\epsilon_0 \begin{bmatrix} \int(\epsilon-\epsilon_1)E_{1,y}E^*_{1,y}\,dx & \int(\epsilon-\epsilon_2)E^*_{1,y}E_{2,y}\,dx \\ \int(\epsilon-\epsilon_1)E_{1,y}E^*_{2,y}\,dx & \int(\epsilon-\epsilon_2)E_{2,y}E^*_{2,y}\,dx \end{bmatrix} \begin{bmatrix} A \\ B \end{bmatrix} \quad (4.31)$$

This system of ordinary differential equations (ODEs) can be written as

$$\begin{aligned} Sd_z\mathbf{A}(z) &= K(z)\mathbf{A}(z) \\ d_z\mathbf{A}(z) &= M(z)\mathbf{A} \end{aligned} \quad (4.32)$$

where $\mathbf{A}(z)^T = [A(z)\ B(z)]$, $M = S^{-1}K$.

- As described in [25], we solve the above system of ODEs using the Runge Kutta Method of order 4.
- Discretise the computational interval $Z = [z_0, z_1]$ in $N+1$ points in the step size of h. Then $z_j = z_0 + j * h$, for $j = 0, 1, 2, \ldots, N$.
- We take advantage of the fact that M is a function of only z, rather than a function of z and $A(z), B(z)$. This is used to form the so called propagation matrices T_j, which relate the discretized amplitude coupling coefficients $\mathbf{A}(z_j)$ to the that of starting values $\mathbf{A}(z_0)$.
- With $T_0 = 1$, the propagation matrices are computed as following

$$\begin{aligned} N_1 &= hM(z_j) \\ N_2 &= hM(z_j + h/2)(1 + N_1/2) \\ N_3 &= hM(z_j + h/2)(1 + N_2/2) \\ N_4 &= hM(z_j + 1)(1 + N_3) \\ T_{j+1} &= (1 + N_1/6 + N_2/3 + N_3/3 + N_4/6)T_j \end{aligned}$$

- Then

$$\mathbf{A}(z_j) = T_j \mathbf{A}(z_0).$$

4.2.4 Scattering Matrix

We have to use the bent coupler model in microring resonator model. For that one must know how the initial amplitudes are related to the final amplitudes. This relationship is given by the scattering matrix. Referring to section 4.1, we can not interpret $A(z)$ and $B(z)$ directly as amplitudes. So the propagation matrix T_j can not be interpreted as the scattering matrix. But appropriate correction of T_j leads to the required scattering matrix S.

Consider the computational setting as shown in the figure 4.2. The coupler is defined in the region $[x_l, x_r] \times [z_{in}, z_{out}]$. In this region TE field is given by

$$E_y(x,z) = A(z)E^0_{1,y}(r(x,z))e^{-i\gamma_1 R\theta(x,z)} + B(z)E^0_{2,y}(x)e^{-i\beta_2 z}$$

where we used a local co-ordinate setting for the ease of argument.

Outside this region, there is a negligible interaction between the two waveguides. Therefore outside the coupler region, the field profile of individual waveguides is same as that of the unperturbed case. For the straight waveguide,

$$E_{2,y}(x,z) = \begin{cases} f(z)\ E^0_{2,y}(x)e^{-i\beta_2(z-z_{in})} & z \le z_{in} \\ F(z)\ E^0_{2,y}(x)e^{-i\beta_2(z-z_{out})} & z \ge z_{out} \end{cases} \tag{4.33}$$

For the bent waveguide,

$$E_{1,y}(r,\theta) = \begin{cases} g(z)\ E^0_{1,y}(r)e^{-i\gamma_1 R(\theta-\theta_{in})} & \theta \le \theta_{in} \\ G(z)\ E^0_{1,y}(r)e^{-i\gamma_1 R(\theta-\theta_{out})} & \theta \ge \theta_{out} \end{cases} \tag{4.34}$$

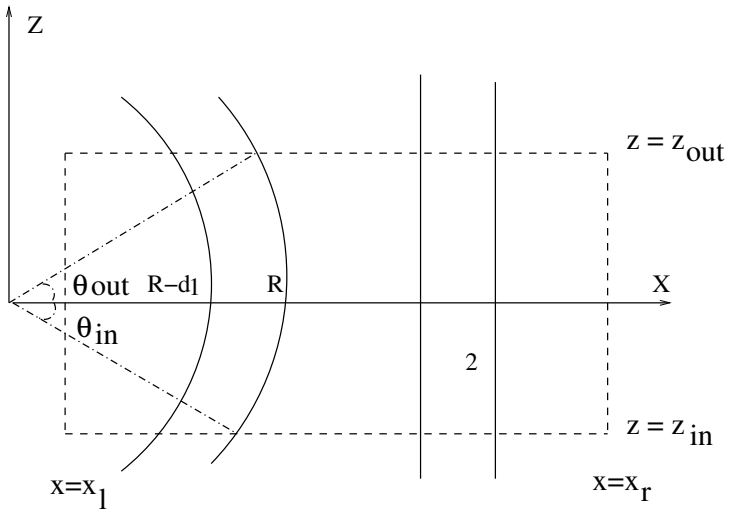

Figure 4.2: Coupler setting

At $z = z_{in}$,

$$\begin{aligned} f(z_{in})\ E^0_{2,y}(x) &= B(z_{in})E_{2,y}(x)^0 e^{-i\beta_2 z_{in}} \\ g(z_{in})\ E^0_{1,y}(r) &= A(z_{in})E^0_{1,y}(r)e^{-i\gamma_1 R\theta_{in}} \end{aligned}$$

Therefore

$$A(z_{in}) = g(z_{in})e^{i\gamma_1 R\theta_{in}} \quad (4.35)$$
$$B(z_{in}) = f(z_{in})e^{-i\beta_2 z_{in}} \quad (4.36)$$

Similarly

$$A(z_{out}) = G(z_{out})e^{i\gamma_1 R\theta_{out}} \quad (4.37)$$
$$B(z_{out}) = F(z_{out})e^{-i\beta_2 z_{out}} \quad (4.38)$$

By knowing the propagation matrix, we have

$$\mathbf{A}(z_{out}) = T_{out}\mathbf{A}(z_{in})$$

Rewrite this equation as

$$\begin{bmatrix} A(z_{out}) \\ B(z_{out}) \end{bmatrix} = \begin{bmatrix} T_{11} & T_{12} \\ T_{21} & T_{22} \end{bmatrix} \begin{bmatrix} A(z_{in}) \\ B(z_{in}) \end{bmatrix}$$

Using eq. (4.35)- (4.38), we get

$$\begin{bmatrix} G(z_{out}) \\ F(z_{out}) \end{bmatrix} = \begin{bmatrix} T_{11}e^{i\gamma_1 R(\theta_{in}-\theta_{out})} & T_{12}e^{i(\beta_2 z_{in}-\gamma_1 R\theta_{out})} \\ T_{21}e^{i(\gamma_1 R\theta_{in}-\beta_2 z_{out})} & T_{22}e^{i\beta_2(z_{in}-z_{out})} \end{bmatrix} \begin{bmatrix} g(z_{in}) \\ f(z_{in}) \end{bmatrix}$$

This gives the scattering matrix S, which relates the input amplitudes $g(z_{in}), f(z_{in})$ with the output amplitudes $G(z_{out}), F(z_{out})$. Let S be given as

$$S = \begin{bmatrix} \rho & \chi \\ \kappa & \tau \end{bmatrix}$$

where

$$\rho = T_{11}e^{i\gamma_1 R(\theta_{in}-\theta_{out})} \quad (4.39)$$
$$\chi = T_{12}e^{i(\beta_2 z_{in}-\gamma_1 R\theta_{out})} \quad (4.40)$$
$$\kappa = T_{21}e^{i(\gamma_1 R\theta_{in}-\beta_2 z_{out})} \quad (4.41)$$
$$\tau = T_{22}e^{i\beta_2(z_{in}-z_{out})} \quad (4.42)$$

The physical interpretation of χ is that it is a measure of coupling from the bent waveguide to the straight waveguide, while κ is a measure of coupling from the straight waveguide to the bent waveguide.

As discussed in [25], we have the following approximate constraints for a lossless coupler:

$$\kappa \approx \chi \quad (4.43)$$
$$|\rho|^2 + |\chi|^2 \approx 1 \quad (4.44)$$
$$|\kappa|^2 + |\tau|^2 \approx 1 \quad (4.45)$$
$$|\rho|^2 \approx |\tau|^2 \approx 1 - |\kappa|^2 \quad (4.46)$$

4.3 Simulation of Bent-Straight Waveguide Coupler

Here we give the numerical results of the simulations of above bend coupler. Our main interests are effects on power transfer of changing radius and changing separation distance. We discuss the numerical results w.r.t. next two settings.

	Case I	Case II
Wavelength [μm]	1.3	1.3
Separation [μm]	2, 1.2, 1, 0.8	1, 0.8, 0.5, 0.4
Bent radius [μm]	500	100
Bent width [μm]	0.5	1
Bent core refractive index	1.61	1.7
Bent background refractive index	1.5	1.58
β_{bend} [μm^{-1}]	7.413958	7.970147
α_{bend} [μm^{-1}]	6.448135e-12	1.312971e-07
Straight waveguide width [μm]	0.5	1
Straight waveguide core refractive index	1.609	1.69
Straight waveguide background refractive index	1.5	1.58
$\beta_{straight}$ [μm^{-1}]	7.414944	7.967143

Table 4.1: Bent coupler simulation settings

Observations

The input is given in the straight waveguide. The simulation results for variation of $|A(z)|^2$ and$|B(z)|^2$ are as shown in figures 4.3 and 4.4.

- Initially most of the power remains in straight waveguide.
- After a certain propagation distance, the bend mode gets excited. The strength and the occurance of power transfer depends upon the separation between two waveguides. Smaller the separation, earlier and more the power transfer.
- The accuracy of the numerical results is checking against the approximate coupler constraints. They agree well.

Case I

Here are the results for large bent radius.

Separation	2 μm	1.2 μm	1.0 μm	0.8 μm
ρ	(0.9417, 0.0621)	(0.3316, 0.1872)	(-0.1367, 0.1078)	(-0.6609, - 0.2401)
τ	(0.9414, - 0.0721)	(0.3758, - 0.0775)	(-0.0543, - 0.1666)	(-0.5636, - 0.4162)
χ	(-0.0225, - 0.3215)	(0.0837, - 0.9045)	(0.2077, - 0.9458)	(0.2865, - 0.6348)
κ	(0.0205, - 0.3375)	(0.2076, - 0.9168)	(0.3392, - 0.9420)	(0.3806, - 0.6211)
$\|\rho\|^2$	0.8907	0.1450	0.0303	0.4944
$\|\tau\|^2$	0.8914	0.1473	0.0307	0.4909
$\|\chi\|$	0.3223	0.9084	0.9683	0.6965
$\|\kappa\|$	0.3382	0.9400	1.0012	0.7284
$\|\rho\|^2 + \|\chi\|^2$	0.9945	0.9702	0.9679	0.9794
$\|\tau\|^2 + \|\kappa\|^2$	1.0057	1.0308	1.0331	1.0215

Table 4.2: Case I: Variation of coupling constants for different separation distances

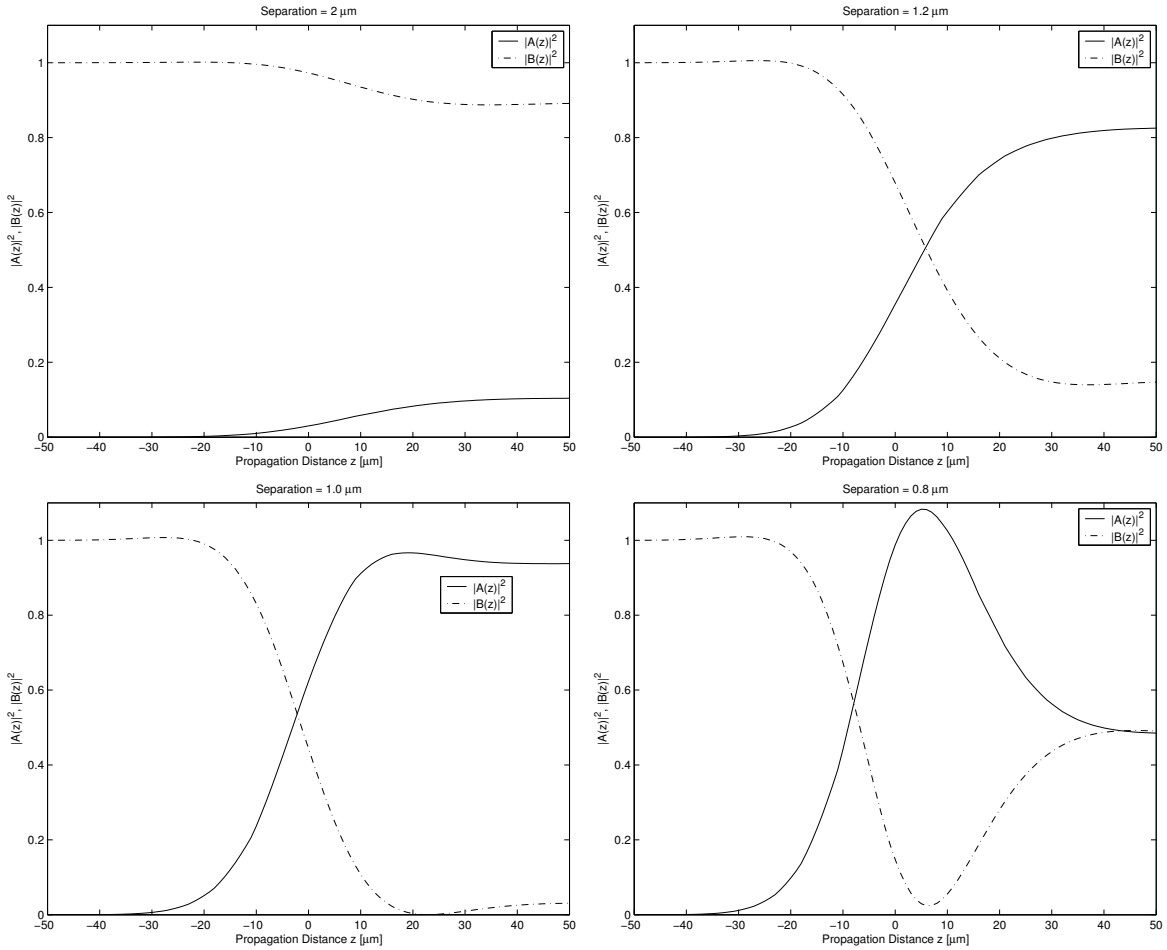

Figure 4.3: Case I: Bend coupler for different separation distances

Case II

The previous analysis is done for smaller radius bent and the results are as follows:

Separation	1.0 μm	0.8 μm	0.5 μm	0.4 μm
ρ	(0.55353, 0.80605)	(0.51877, 0.79210)	(0.38407,0.71110)	(0.28740, 0.62127)
τ	(0.30858, 0.92939)	(0.29927,0.89965)	(0.26057, 0.76601)	(0.23250, 0.64411)
χ	(0.19440, - 0.084436)	(0.30524, - 0.12872)	(0.58841, - 0.22160)	(0.71313, - 0.25092)
κ	(0.16951, -0.093869)	(0.26774, -0.14539)	(0.49077, - 0.24329)	(0.63449,- 0.29786)
$\lvert\rho\rvert^2$	0.95611	0.89653	0.65317	0.46857
$\lvert\tau\rvert^2$	0.95899	0.89892	0.65468	0.46894
$\lvert\chi\rvert$	0.21194	0.33127	0.62875	0.75599
$\lvert\kappa\rvert$	0.19377	0.30467	0.54777	0.70093
$\lvert\rho\rvert^2 + \lvert\chi\rvert^2$	1.0010	1.0063	1.0485	1.0401
$\lvert\tau\rvert^2 + \lvert\kappa\rvert^2$	0.99654	0.99175	0.95472	0.96024

Table 4.3: Case II: Variation of coupling constants for different separation distances

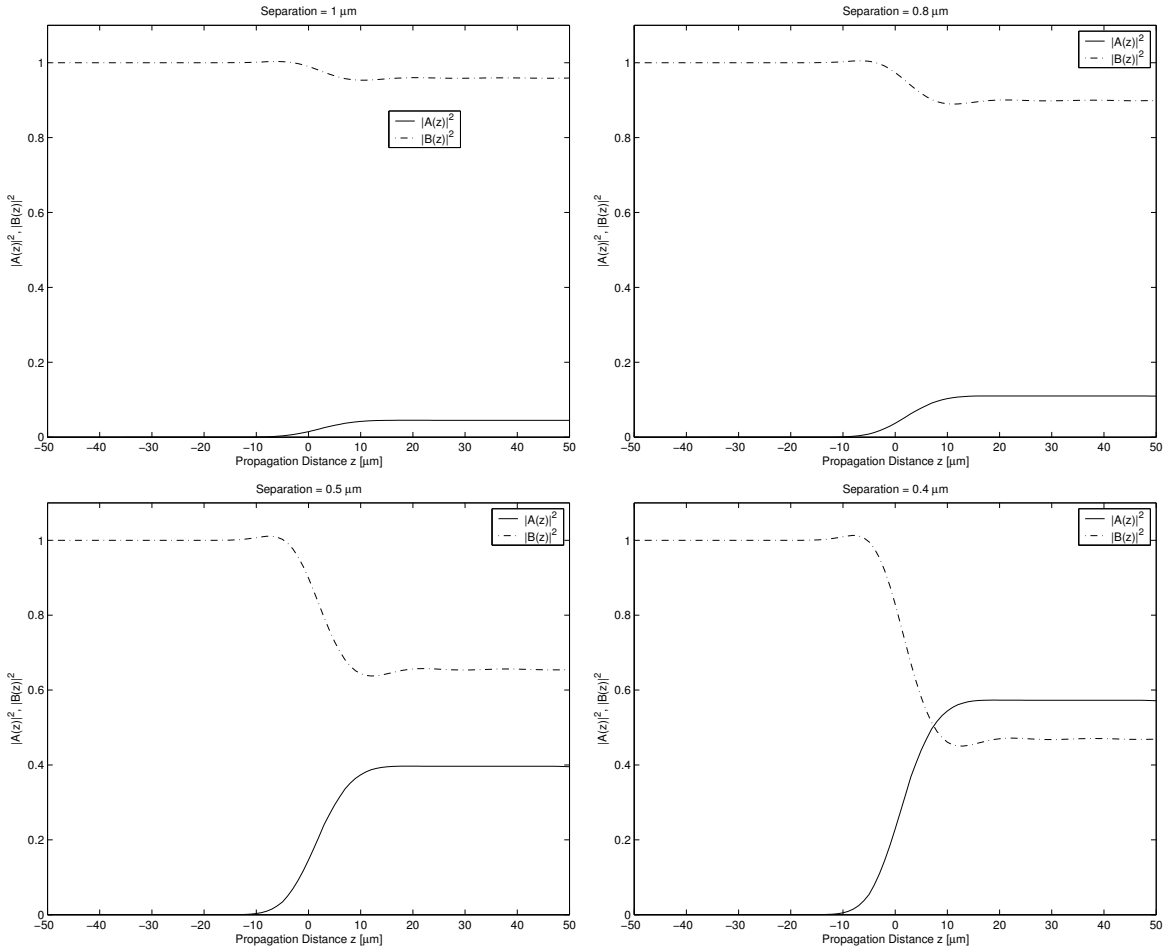

Figure 4.4: Case II: Bend coupler for different separation distances

Chapter 5

Modeling of Microring Resonators

The concepts in this section are based on the reference [26]. The microring resonator model is based on the following approximations.

- All the waveguides are mono mode.
- Only single polarized modes are considered.
- Inside the coupler and microring back reflections are negligible.
- Outside the coupler region, there is negligible interaction between the two waveguides.
- All elements are completely linear.

5.1 Microring Resonator Model

The schematic diagram of the microring resonator under consideration is as follows.

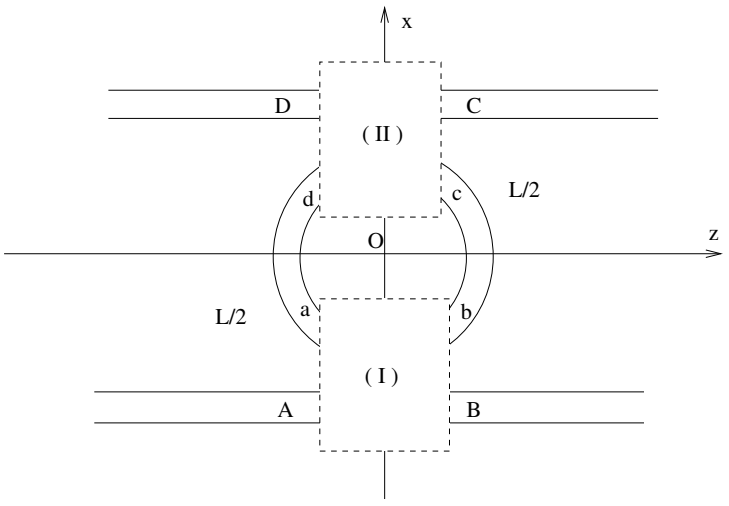

Figure 5.1: Microring resonator model in terms of bend couplers

The microring resonator consists of two bent couplers (coupler I and coupler II), two bend waveguides (of length $L/2$) and four external ports made up of straight waveguides. Variables $A_{\pm}, B_{\pm}, C_{\pm}, D_{\pm}$ (external connections) and $a_{\pm}, b_{\pm}, c_{\pm}, d_{\pm}$ (cavity connections) denote the amplitudes of the guided modes

in the coupler port planes which are identified by corresponding letters. The sign ± correspond to modes traveling in either positive or negative z direction.

The relationship between coupler input and output amplitudes is given by following scattering matrix

$$\begin{bmatrix} A_- \\ a_- \end{bmatrix} = \begin{bmatrix} \rho & \chi \\ \kappa & \tau \end{bmatrix} \begin{bmatrix} B_- \\ b_- \end{bmatrix} \qquad \begin{bmatrix} B_+ \\ b_+ \end{bmatrix} = \begin{bmatrix} \rho & \chi \\ \kappa & \tau \end{bmatrix} \begin{bmatrix} A_+ \\ a_+ \end{bmatrix} \tag{5.1}$$

Similarly

$$\begin{bmatrix} D_- \\ d_- \end{bmatrix} = \begin{bmatrix} \rho & \chi \\ \kappa & \tau \end{bmatrix} \begin{bmatrix} C_- \\ c_- \end{bmatrix} \qquad \begin{bmatrix} C_+ \\ c_+ \end{bmatrix} = \begin{bmatrix} \rho & \chi \\ \kappa & \tau \end{bmatrix} \begin{bmatrix} D_+ \\ d_+ \end{bmatrix} \tag{5.2}$$

ρ and τ are known as *self coupling coefficients*, χ and κ are known as *cross coupling coefficients*. The physical interpretation of χ is that it is a measure of coupling from the bent waveguide to the straight waveguide, while κ is a measure of coupling from the straight waveguide to the bent waveguide. For approximate lossless couplers

$$\kappa \approx \chi \tag{5.3}$$
$$|\rho|^2 + |\chi|^2 \approx 1 \tag{5.4}$$
$$|\kappa|^2 + |\tau|^2 \approx 1 \tag{5.5}$$
$$|\rho|^2 \approx |\tau|^2 \approx 1 - |\kappa|^2 \tag{5.6}$$

Let $\gamma = \beta - i\alpha$ be the bent propagation constant. Then

$$c_- = b_+ \exp(-i\beta L/2) \exp(-\alpha L/2) \tag{5.7}$$
$$a_+ = d_- \exp(-i\beta L/2) \exp(-\alpha L/2) \tag{5.8}$$
$$b_- = c_+ \exp(-i\beta L/2) \exp(-\alpha L/2) \tag{5.9}$$
$$d_+ = a_- \exp(-i\beta L/2) \exp(-\alpha L/2) \tag{5.10}$$

5.2 Transfer Characteristics

Given a power input at A_+, we are interested in the transmitted power at B_+ and the backwards dropped power at D_-. Given an excitation in only one of the external ports $A_+ = \sqrt{P_{in}}, B_- = D_+ = C_- = 0$, eq. 5.1, 5.2, 5.7 -5.10 are solved for transmitted power $P_T = |B_+|^2$ and the backwards dropped power $P_D = |D_-|^2$, with the assumption no back reflected power $A_- = 0$ and no forward dropped power $C_+ = 0$. This gives

$$D_- = \frac{\chi\kappa p}{1 - \tau^2 p^2} A_+, \qquad B_+ = \left(\rho + \frac{\chi\kappa\tau p^2}{1 - \tau^2 p^2}\right) A_+ \tag{5.11}$$

where $p = \exp(-i\beta L/2) \exp(-\alpha L/2)$. Let $\tau = |\tau| \exp(i\varphi)$. Then

$$P_D = P_{in} \frac{|\kappa|^2 |\chi|^2 \exp(-\alpha L)}{1 + |\tau|^4 \exp(-2\alpha L) - 2|\tau|^2 \exp(-\alpha L) \cos(\beta L - 2\varphi)} \tag{5.12}$$

$$P_T = P_{in} \frac{|\rho|^2 (1 + |\tau|^2 d^2 \exp(-2\alpha L) - 2|\tau| d \exp(-\alpha L) \cos(\beta L \varphi - \psi))}{1 + |\tau|^4 \exp(-2\alpha L) - 2|\tau|^2 \exp(-\alpha L) \cos(\beta L - 2\varphi)} \tag{5.13}$$

where $\tau - \chi\kappa/\rho = d \exp(i\psi)$ with d and ψ real.

5.3 Resonances

Resonances appears as maxima of the dropped power P_D and minima of the transmitted power P_T. From eq. (5.12), the maxima of the dropped power is characterised by the condition $\cos(\beta L - 2\varphi) = 1$. i.e.

$$\beta = \frac{2m\pi + 2\varphi}{L} =: \beta_m, \text{for integer } m \tag{5.14}$$

At resonance, the dropped power is given by

$$P_D|_{\beta=\beta_m} = P_{in}\frac{|\kappa|^2|\chi|^2\exp(-\alpha L)}{(1-|\tau|^2\exp(-\alpha L))} \tag{5.15}$$

While in principle, all the quantities that describe the behavior of the directional coupler and of the ring loops are wavelength dependent, as a first order approximation, we assume that only the ring propagation constant is wavelength dependent and the scattering matrix remains constant in sufficiently small wavelength range. Here we quote the results for important resonator related quantities from [26]. The *free spectral range* (FSR), the distance between to successive maxima's of dropped power, is given by

$$\Delta\lambda \approx \left.\frac{\lambda^2}{n_{eff}L}\right|_m \tag{5.16}$$

The above expression gives FSR around the resonance of order m, $n_{eff} = \lambda\beta_m/(2\pi)$.

The *full width at half maximum* (FWHM), which is a measure of the wavelength region in which power drops to half of the resonance value, is given by

$$2\delta\lambda \approx \left.\frac{\lambda^2}{\pi n_{eff}L}\right|_m \left(\frac{1}{|\tau|}\exp(\alpha L/2) - |\tau|\exp(-\alpha L/2)\right) \tag{5.17}$$

The finess (F) of the resonator, which is defined as a ratio of FSR and FWHM, is given by

$$F = \frac{\Delta\lambda}{2\delta\lambda} = \pi\frac{|T|\exp(-\alpha L/2)}{1-|T|^2\exp(-\alpha L)} \tag{5.18}$$

The Q-factor, which is defined as the ratio of the operation wavelength and FWHM, is given by

$$Q = \frac{\lambda}{2\delta\lambda} = \frac{n_{eff}L}{\lambda}F \tag{5.19}$$

5.4 Simulation of Microring Resonators

Here we present the simulation results of above model with the following approximations.

- We assume that $\chi = \kappa$ in the following simulations. We generally take it equal to the average value of the computed values of χ and κ.
- In a sufficiently small neighborhood of a given wavelength, we take the scattering matrix constant.
- Arguing with the approximation that only the ring propagation constant is wavelength dependent and using the values of the scattering matrix given at the central frequency, we calculate the power dropped P_D and the power transmitted P_T using eq. (5.12), (5.13).

Consider the settings inn the section 4.3.

- Case I with separation = 0.8 μm
- Case II with separation = 0.5 μm

Specific values of waveguide parameters are given in table 4.1. The values of coupling coefficients at the central frequency $\lambda = 1.3\mu m$ are given in table 4.2 and 4.3.

This gives transfer characteristics of the resonator as shown in figure 5.2 and 5.3. We see that there is a periodic power drop and power transmission.

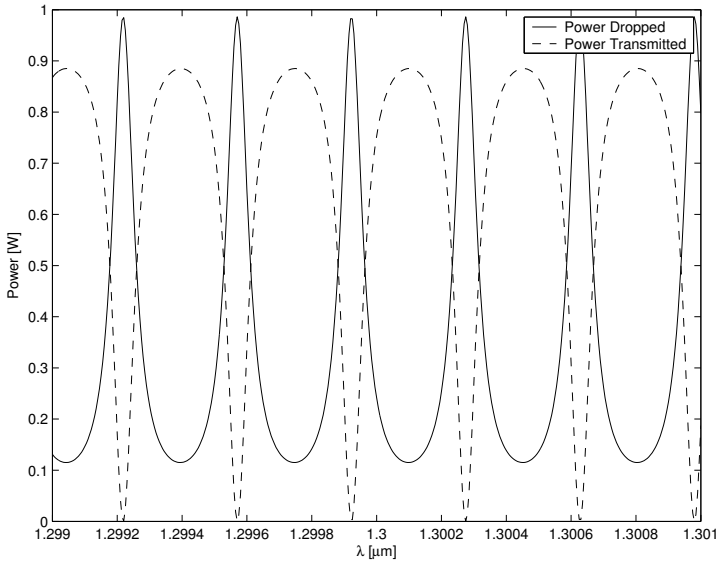

Figure 5.2: Case I with separation=0.8 μm.

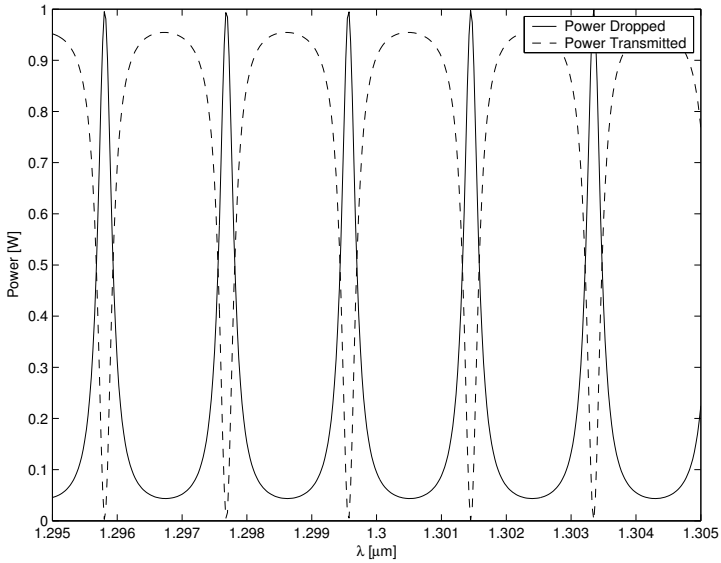

Figure 5.3: Case II with separation=0.5 μm.

Chapter 6

Conclusions

6.1 Conclusions

- In this work, we attempted a modeling of a microresonator based on spatial couple mode theory. This model uses the modes of a straight waveguide and a bent waveguide.
- A bent waveguide model is developed and a semi analytical bent mode solver is implemented.
- For small bent radius, bent modal field is radiative in the cover region and the maximum is close to core-cover interface. As bent radius increases, this radiation effect decreases. For the small bent radius, the phase profile in cover region is curved. As bent radius increases, it becomes plane, similar to that of equivalent straight waveguide.
- As the bent radius increases, $\beta_{bent} \longrightarrow \beta_{straight}$. For *sufficiently* large radius, $\frac{\alpha}{k_0} \propto e^{-c_1 R}$, where c_1 is an unknown constant.
- Using these bent modes, a model of coupler consisting of a bent waveguide and a straight waveguide is presented. The simulation results of approximately lossless coupler satisfy the (approximate) coupler constraints.
- A microresonator is modeled in terms of a coupler involving a bent waveguide and a straight waveguide. This model is simulated. The microresonator simulations show typical maxima's for power dropped and minima's for power transmitted.

6.2 Acknowledgment

I enjoyed working on this subject. I am thankful to my supervisor Manfred Hammer and his patience to convince me. His *"Be precise Kiran"* helped me a lot. Brenny van Groesen's simple questions during discussions kept me busy for weeks. He inspired me to look at the same problem from different aspects. I also acknowledge the day-today help from the colleagues at Department of Mathematics to solve innumerable problems now-and-then. I thank them. Still I have to improve a lot. All I feel at this moment is,

"*A journey has just began.....*"

Appendix A

Maxwell Equations

An optical waveguide is a device which guides the optical signals from one point to another. It's mathematical model is based on Maxwell equations for electromagnetic waves with the relevant interface conditions. The operational wavelength range is 0.1 μm to 10 μm (corresponding to frequency $10^3 - 10^5$ Å), which is determined by the available laser frequencies and material properties like regions of transparency of optical fibers. For wavelengths much larger than 10 μm, metallic waveguide techniques are employed. For wavelengths less than 0.1 μm, there are high scattering and absorption losses. The operational refractive index range is 1 (for air) to 3.6 (for $GaAs$ at $\lambda = 0.9$ μm) [50, pp.1].

Maxwell Equations

Maxwell equations are the fundamental equations of electrodynamics which describe all macroscopic electromagnetic phenomena [12]. In the most general differential and integral form, these equations are as

$\nabla \times \mathbf{E} = -\frac{d\mathbf{B}}{dt}$	$\oint_C \mathbf{E} \cdot dl = -\frac{d\Phi}{dt}$	Faraday's law
$\nabla \times \mathbf{H} = \mathbf{J} + \frac{d\mathbf{D}}{dt}$	$\oint_C \mathbf{H} \cdot dl = I + \int_S \frac{d\mathbf{D}}{dt} \cdot d\mathbf{s}$	Ampere's circuital law
$\nabla \cdot \mathbf{D} = \rho$	$\oint_S \mathbf{D} \cdot d\mathbf{s} = Q$	Gauss's law
$\nabla \cdot \mathbf{B} = 0$	$\oint_B \mathbf{D} \cdot d\mathbf{s} = 0$	No isolated magnetic charge

For a linear isotropic material, we have the following important constitutive relations:

$$\begin{aligned} \mathbf{D} &= \epsilon_0 \epsilon \mathbf{E} \\ \mathbf{H} &= \frac{\mathbf{B}}{\mu_0 \mu} \end{aligned}$$

where,

$\mathbf{E}$ = Electric field (V/m)	$\mathbf{B}$ = Magnetic flux density (T)
$\mathbf{H}$ = Magnetic field(A/m)	$\mathbf{D}$ = Electric flux density / dielectric displacement(C/m^2)
$\mathbf{J}$ = Volume current density(A/m^2)	ρ = Volume free charge density(C/m^3)
ϵ_0 = Vacuum permittivity(F/m)	ϵ = Relative permittivity
μ_0 = Vacuum permeability(H/m)	μ = Relative permeability
Q = Total charge(C)	Φ = Magnetic flux(Wb)

To describe the propagation of electromagnetic waves in a structure involving contiguous regions of different constitutive parameters (ϵ and μ), one needs to know the conditions for $\mathbf{E}$, $\mathbf{D}$, $\mathbf{B}$, $\mathbf{H}$ at the

interfaces. These conditions are known as *boundary conditions* or *interface conditions*. Using the integral form of Maxwell equations, we get following interface relationships of the *tangential components of fields (***E** *or* **H***)* and the *normal components of fluxes (***D** *or* **B***).*

General Interface Conditions for Electromagnetic field

Using the integral form of Maxwell equations, we get the following general interface conditions.

1. The tangential component of the **E** field is continuous across an interface.

$$\mathbf{a}_n \times \mathbf{E}_1 = \mathbf{a}_n \times \mathbf{E}_2$$

   where $\mathbf{a}_n$ is outward unit normal to the interface .

2. The normal component of the **D** field is discontinuous across an interface, where surface charges exist. The amount of discontinuity is equal to the surface charge density.

$$\mathbf{a}_n \cdot (\mathbf{D}_1 - \mathbf{D}_2) = \rho_s$$

3. The tangential component of the **H** field is discontinuous across an interface, where surface currents exist. The amount of discontinuity is equal to the surface current density on the interface normal to the contour.

$$\mathbf{a}_n \times (\mathbf{H}_1 - \mathbf{H}_2) = \mathbf{J}_s$$

4. The normal component of **B** field is continuous across an interface.

$$\mathbf{a}_n \cdot \mathbf{B}_1 = \mathbf{a}_n \cdot \mathbf{B}_2$$

Simplification for a Source Free Media

In the present case, we are considering dielectric ($\mathbf{J} = 0$), source free ($\rho = 0$), linear, isotopic, non magnetic ($\mu = \mu_0$), transparent materials. For this case Maxwell equations become

$$\nabla \times \mathbf{E} = -\mu_0 \frac{d\mathbf{H}}{dt} \tag{A.1}$$

$$\nabla \times \mathbf{H} = \epsilon_0 \epsilon \frac{d\mathbf{E}}{dt} \tag{A.2}$$

$$\nabla \cdot (\epsilon \mathbf{E}) = 0 \tag{A.3}$$

$$\nabla \cdot \mathbf{H} = 0 \tag{A.4}$$

where ϵ is dielectric constant (also known as relative permittivity and often denoted by ϵ_r). note that $\sqrt{\epsilon} = n$, where n is refractive index of the corresponding medium. The physical field is the real part of **E** and **H**.

For a source free medium ($\rho_s = 0$), dielectric ($J_s = 0$), interface conditions become,

$$\mathbf{E}_{1t} = \mathbf{E}_{2t} \qquad \epsilon_1 \mathbf{E}_{1n} = \epsilon_2 \mathbf{E}_{2n} \qquad \mathbf{H}_{1t} = \mathbf{H}_{2t} \qquad \mathbf{H}_{1t} = \mathbf{H}_{2t}$$

where subscript t denotes tangential component and subscript n denotes normal component.
Taking curl of eq. (A.1) and simplifying

$$\nabla \times \nabla \times \mathbf{E} + \mu_0 \epsilon_0 \epsilon \frac{\partial^2 \mathbf{E}}{\partial t^2} = 0$$

This is a wave equation for source free medium.

Appendix B

Bessel Equation

The governing wave equation for the y component of $\mathbf{E}$ in the cylindrical co-ordinates reduces to the Bessel equation. The general form of the Bessel equation is

$$x^2\frac{d^2y}{dx^2} + x\frac{dy}{dx} + (x^2 - \nu^2)y = 0$$

In our case, $x \in \mathbb{R}$, $\nu \in \mathbb{C}$ and $y(x)$ is a complex valued function.
Its general solution is a linear combination of Bessel function of the first kind $J_\nu(x)$ and Bessel function of the second kind $Y_\nu(x)$.

$$y(x) = c_1 J_\nu(x) + c_2 Y_\nu(x)$$

where

$$\begin{aligned} J_\nu(x) &= \sum_{k=0}^{\infty} \frac{(-1)^k (x/2)^{\nu+2k}}{k!\Gamma(\nu + k + 1)}, \\ Y_\nu(x) &= \frac{J_\nu(x)\cos(\nu\pi) - J_{-\nu}(x)}{\sin(\nu\pi)}, \end{aligned}$$

where $Y_\nu(x)$ is the second linearly independent solution.
For the study of wave phenomena, it is convenient to define a Hankel function of the first kind $H_\nu^{(1)}(x)$ and a Hankel function of the second kind $H_\nu^{(2)}(x)$ as

$$\begin{aligned} H_\nu^{(1)}(x) &= J_\nu(x) + iY_\nu(x), \\ H_\nu^{(2)}(x) &= J_\nu(x) - iY_\nu(x). \end{aligned}$$

Then the above solution can also be written as

$$y(x) = d_1 H_\nu^{(1)}(x) + d_2 H_\nu^{(2)}(x),$$

where c_1, c_2, d_1, d_2 are arbitrary constants.

Principal Asymptotic Forms

For fixed ν and $|x| \longrightarrow \infty$, the principal asymptotic form of Hankel functions is given by [1, chap. 9]

$$H_\nu^{(1)}(x) \approx \sqrt{\frac{2}{\pi x}} e^{i(x - \frac{1}{2}\nu\pi - \frac{1}{4}\pi)} \qquad (-\pi < \arg x < 2\pi) \tag{B.1}$$

$$H_\nu^{(2)}(x) \approx \sqrt{\frac{2}{\pi x}} e^{-i(x - \frac{1}{2}\nu\pi - \frac{1}{4}\pi)} \qquad (-2\pi < \arg x < \pi) \tag{B.2}$$

Useful Formulas

Here are few useful identities involving Bessel functions and Hankel functions.

$$J_\nu^{'}(x) = \frac{1}{2}\left[J_{\nu-1}^{'}(x) - J_{\nu+1}^{'}(x)\right] \tag{B.3}$$

$$Y_\nu^{'}(x) = \frac{1}{2}\left[Y_{\nu-1}^{'}(x) - Y_{\nu+1}^{'}(x)\right] \tag{B.4}$$

$$H_\nu^{(2)'}(x) = \frac{1}{2}\left[H_{\nu-1}^{(2)'}(x) - H_{\nu+1}^{(2)'}(x)\right] \tag{B.5}$$

Appendix C

Implementation of Complex Order Bessel Functions

Introduction

For bend mode solver, we need to evaluate complex order and real argument bessel functions and Hankel functions. The author found that the routines for computation of complex order Bessel functions are not available as easily as compared to that of real order Bessel functions. MATLAB has complex argument but real order Bessel function routines. MAPLE has complex argument and complex order routine, but it takes much computation time for high orders. In the investigation of bend modes, there was a need of fast routine for complex order Bessel functions. We undertook this task.

Remark: We are basically interested in complex order and real argument Bessel routines. Here after, Bessel functions means Bessel functions of complex order and real argument.

Method

There are different methods available for the computation of complex order and real argument Bessel functions. Depending upon the method, the complexity and the accuracy of the computation varies. We were primarily interested in large complex order Bessel functions. One of the methods suitable for this category is *"Uniform Asymptotic Expansions"* of Bessel functions in terms of Airy functions[1, chap. 9].

Expansion for Bessel functions

Case : Order $\neq$ Argument

$$J_\nu(\nu z) \sim \left(\frac{4\zeta}{1-z^2}\right)^{1/4} \left\{ \frac{Ai(\nu^{2/3}\zeta)}{\nu^{1/3}} \sum_{k=0}^{\infty} \frac{a_k(\zeta)}{\nu^{2k}} + \frac{Ai'(\nu^{2/3}\zeta)}{\nu^{5/3}} \sum_{k=0}^{\infty} \frac{b_k(\zeta)}{\nu^{2k}} \right\}, \tag{C.1}$$

$$Y_\nu(\nu z) \sim -\left(\frac{4\zeta}{1-z^2}\right)^{1/4} \left\{ \frac{Bi(\nu^{2/3}\zeta)}{\nu^{1/3}} \sum_{k=0}^{\infty} \frac{a_k(\zeta)}{\nu^{2k}} + \frac{Bi'(\nu^{2/3}\zeta)}{\nu^{5/3}} \sum_{k=0}^{\infty} \frac{b_k(\zeta)}{\nu^{2k}} \right\}. \tag{C.2}$$

The parameter ζ is defined as

$$\begin{array}{lcll} \frac{2}{3}\zeta^{3/2} & = & \ln\frac{1+\sqrt{1-z^2}}{z} - \sqrt{1-z^2}, & 0 \le z \le 1, \\ \frac{2}{3}(-\zeta)^{3/2} & = & \sqrt{z^2-1} - \arccos\frac{1}{z}, & z \ge 1. \end{array} \tag{C.3}$$

$Ai(\cdot)$ and $Bi(\cdot)$ are Airy functions, (also denoted as $AiryAi(\cdot)$ and $AiryBi(\cdot)$). The functions $a_k(\cdot)$ and $b_k(\cdot)$ are given by

$$a_k(\zeta) = \sum_{s=0}^{2k} \mu_s \zeta^{-3s/2} u_{2k-s}\{(1-z^2)^{-1/2}\}, \tag{C.4}$$

$$b_k(\zeta) = -\zeta^{-1/2} \sum_{s=0}^{2k+1} \lambda_s \zeta^{-3s/2} u_{2k-s+1}\{(1-z^2)^{-1/2}\}, \tag{C.5}$$

where μ_s and λ_s are given by

$$\lambda_s = \frac{(2s+1)(2s+3)\cdots(6s-1)}{s!(144)^s}, \tag{C.6}$$

$$\mu_s = -\frac{6s+1}{6s-1}\lambda_s, \tag{C.7}$$

and u_k are given by

$$u_0(t) = 1, \tag{C.8}$$

$$u_1(t) = \frac{3t-5t^3}{24}, \tag{C.9}$$

$$u_2(t) = \frac{81t^2-462t^4+385t^6}{1152}, \tag{C.10}$$

$$\vdots \quad \vdots \quad \vdots \tag{C.11}$$

$$u_{k+1}(t) = \frac{1}{2}t^2(1-t^2)u_k^{'}(t) + \frac{1}{8}, \int_0^t (1-5t^2)u_k(t)dt, \qquad (k=0,1,\cdots). \tag{C.12}$$

Case : Order = Argument

When order of the Bessel functions is equal to its argument, then clearly above expansions do not hold true. In this case, we use the following expansions.

$$J_\nu(\nu) \sim \frac{a}{\nu^{1/3}}\{1+\sum_{k=1}^{\infty}\frac{\alpha_k}{\nu^{2k}}\} - \frac{b}{\nu^{5/3}}\sum_{k=0}^{\infty}\frac{\beta_k}{\nu^{2k}} \tag{C.13}$$

$$Y_\nu(\nu) \sim -\frac{\sqrt{3}a}{\nu^{1/3}}\{1+\sum_{k=1}^{\infty}\frac{\alpha_k}{\nu^{2k}}\} - \frac{\sqrt{3}b}{\nu^{5/3}}\sum_{k=0}^{\infty}\frac{\beta_k}{\nu^{2k}} \tag{C.14}$$

where

$$a = 0.44730\ \ 73184 \qquad b = 0.41085\ \ 01939$$

$$\alpha_0 = 1 \qquad \alpha_1 = -0.004 \qquad \alpha_2 = 0.00069\ \ 3735\ldots \qquad \alpha_3 = -0.00035\ \ 38\ldots$$

$$\beta_0 = 0.01428\ \ 57143\ldots \qquad \beta_1 = -0.00118\ \ 48596\ldots \qquad \beta_2 = 0.00043\ \ 78\ldots \qquad \beta_3 = -0.00038\ldots$$

Expansion for derivative of Bessel functions

Case: Order $\neq$ Argument

We are also interested in the first order derivative w.r.t. argument of the Bessel function. They are given by

$$J_\nu^{'}(\nu z) \sim -\frac{2}{z}\left(\frac{1-z^2}{4\zeta}\right)^{1/4}\left\{\frac{Ai(\nu^{2/3}\zeta)}{\nu^{4/3}}\sum_{k=0}^{\infty}\frac{c_k(\zeta)}{\nu^{2k}} + \frac{Ai^{'}(\nu^{2/3}\zeta)}{\nu^{2/3}}\sum_{k=0}^{\infty}\frac{d_k(\zeta)}{\nu^{2k}}\right\}, \tag{C.15}$$

$$Y_\nu^{'}(\nu z) \sim \frac{2}{z}\left(\frac{1-z^2}{4\zeta}\right)^{1/4}\left\{\frac{Bi(\nu^{2/3}\zeta)}{\nu^{4/3}}\sum_{k=0}^{\infty}\frac{c_k(\zeta)}{\nu^{2k}} + \frac{Bi^{'}(\nu^{2/3}\zeta)}{\nu^{2/3}}\sum_{k=0}^{\infty}\frac{d_k(\zeta)}{\nu^{2k}}\right\}, \tag{C.16}$$

where,

$$c_k(\zeta) = -\sqrt{\zeta}\sum_{s=0}^{2k+1}\mu_s\zeta^{-3s/2}v_{2k-s+1}\{(1-z^2)^{-1/2}\}, \quad (C.17)$$

$$d_k(\zeta) = \sum_{s=0}^{2k}\lambda_s\zeta^{-3s/2}v_{2k-s}\{(1-z^2)^{-1/2}\}, \quad (C.18)$$

and v_k are given by

$$v_0(t) = 1, \quad (C.19)$$

$$v_1(t) = \frac{-9t+7t^3}{24}, \quad (C.20)$$

$$v_2(t) = \frac{-135t^2+594^4-455^6}{1152}, \quad (C.21)$$

$$\vdots \quad \vdots \quad \vdots \quad (C.22)$$

$$v_{k+1}(t) = u_k(t) + t(t^2-1)\{\frac{1}{2}u_{k-1}(t) + tu_{k-1}^{'}(t)\}, \quad (k=1,2,\cdots). \quad (C.23)$$

Case: Order = Argument

When order of the Bessel functions is equal to its argument, then expansions for derivatives are given as

$$J_\nu^{'}(\nu) \sim \frac{b}{\nu^{2/3}}\{1+\sum_{k=1}^{\infty}\frac{\gamma_k}{\nu^{2k}}\} - \frac{a}{\nu^{4/3}}\sum_{k=0}^{\infty}\frac{\delta_k}{\nu^{2k}} \quad (C.24)$$

$$Y_\nu^{'}(\nu) \sim \frac{\sqrt{3}b}{\nu^{2/3}}\{1+\sum_{k=1}^{\infty}\frac{\gamma_k}{\nu^{2k}}\} + \frac{\sqrt{3}a}{\nu^{5/3}}\sum_{k=0}^{\infty}\frac{\delta_k}{\nu^{2k}} \quad (C.25)$$

where

$$a = 0.44730\ \ 73184 \qquad b = 0.41085\ \ 01939$$

$$\gamma_0 = 1, \qquad \gamma_1 = 0.00730\ \ 15873\ldots \qquad \gamma_2 = -0.00093\ \ 7300\ldots \qquad \gamma_3 = 0.00044\ \ 40\ldots$$

$$\delta_0 = 0.2, \qquad \delta_1 = -0.00273\ \ 30447\ldots \qquad \delta_2 = -0.00060\ \ 47\ldots \qquad \delta_3 = 0.00038\ldots$$

Implementation

- Due to availability of built in complex data type and object oriented features, C++ was natural choice for the coding language.
- Use of propritory sofware routines (e.g. NAG routines) was intentioinaly avoided.
- To avoid the reinventing the wheel, it was decided to use already developed and well tested routines for complex Airy functions. For this, we used the complex Airy functions routines developed by Donald E. Amos and downloaded from `www.netlib.org`.
- Since the Airy function routines were available in FORTRAN 77, this choice lead to using FORTRAN 77 code within C++ code. This interfacing is little bit tricky and compiler dependent, but much more reliable and time saving compared to inventing new wheel!

Bibliography

[1] M. Abramowitz and I. A. Stegun. *Handbook of Mathematical Functions(Applied Mathematics Series 55)*. NBS, Washington, D. C., 1964.

[2] P. P. Absil, J. V. Hryniewicz, B. E. Little, F. G. Johnson, K. J. Ritter, and P. T. Ho. Vertically coupled microring resonators using polymer wafer bonding. *IEEE Photonics Technology Letters*, 13(1):49–51, 2001.

[3] M. L. M. Balistreri, D. J. W. Klunder, F. C. Blom, A. Driessen, J. P. Korterik, L. Kuipers, and N. F. van Hulst. Experimental analysis of the whispering gallery modes in a cylinderical optical microcavity. *J. Opt. Soc. Am. B*, 18(4):465–471, April 2001.

[4] M. L. M. Balistreri, D. J. W. Klunder, F.C. Blom, A. Driessen, H. W. J. M. Hoekstra, J. P. Korterik, L. Kuipers, and N. F. van Hulst. Visualizing the whispering gallery modes in a cylindrical optical microcavity. *Optics Letters*, 24(24):1829–1831, 1999.

[5] H. J. M. Bastiaansen. *Modal Analysis of Straight and Curved Integrated Optical Waveguides, An integral equation approch*. PhD thesis, Delft University, The Netherlands, 1994.

[6] F. C. Blom, H. Kelderman, H. J. W. M. Hoekstra, A. Driessen, and T. J. A. Popma. Experimental study of integrated optics microcavity resonators: Towards and all optical switching device. *Applied Physics Letter*, 71:747–749, 1997.

[7] F. C. Blom, H. Kelderman, H. W. J. M. Hoekstra, A. Driessen, Th. J. A. Popma, S. T. Chu, and B. E. Little. A single channel dropping filter based on a cylindrical microresonator. *Optics Communications*, 167:77–82, 1999.

[8] Freek C. Blom. *Linear and non linear optical properties of cylindrical microresonators-From material to device realisation*. PhD thesis, University of Twente, Enschede, The Nehterlands, 1998.

[9] S. V. Boriskina and A. I. Nosich. Radiation and absorption losses of the whispering gallery mode dielectric resonators excited by a dielectric waveguide. *IEEE Trans. Microwave Theory and Techniques*, 47(2):224–231, 1999.

[10] Ming Cai and Kerry Vahala. Highly efficient optical power transfer to whispering gallery modes by the use of the symmetrical dual coupling configuration. *Optics Letters*, 25(4):260–262, February 2000.

[11] Lewin Chang and Kuester. *Electromagnetic Waves and Curved Structures*. Peter Peregrinus Ltd. (On behalf of IEE), Southgate House, Stevenage, Herts, SG1 1HQ, England, 1977.

[12] David K. Cheng. *Fields and Wave Electromagnetcs (2'nd Ed.)*. Addison-Wesley, U.S.A., 1989.

[13] M. K. Chin, D. Y. Chu, and S. T. Ho. Estimation of the spontaneous emission factor for microdisk lasers via the approximation of whispering gallery modes. *J. Appl. Phys.*, 75:3302–3307, April 1994.

[14] M. K. Chin and S. T. Ho. Design and modeling of waveguide coupled single mode microring resonator. *IEEE J. Lightwave Technology*, 16(8):1433–1446, 1998.

[15] J. M. Choi, R. K. Lee, and Amnon Yariv. Control of critical coupling in a ring resonator fiber configuration: Application to wavelength selective switching, modulation, amplification and oscillation. *Optics Letters*, 26(16):1236–1238, August 2001.

[16] J. M. Choi, R. K. Lee, and Amnon Yariv. Ring fiber resonators based on fused fiber grating add drop filters: Application to resonator coupling. *Optics Letters*, 27(18):1598–1600, September 2002.

[17] L. Djaloshinski and M. Orenstein. Disk and ring microcavity lasers and their concentric coupling. *IEEE J. Quantum Electronics*, 35(5):737–744, 1999.

[18] K. Djordjev, S. J. Choi, S. J. Choi, and P. D. Dapkus. Active semiconductor microdisk devices. *IEEE J. Lightwave Technology*, 20(1):105–113, 2002.

[19] K. Djordjev, S. J. Choi, S. J. Choi, and P. D. Dapkus. Study of effects of the geometry on the performance of vertically coupled InP microdisk resonators. *IEEE J. Lightwave Technology*, 2002. (to be appear).

[20] M. K. Gonokami, R. H. Jordan, A. Dodabalapur, H. E. Katz, M. L. Schilling, and R. E. Slusher. Polymer microdisk and microring lasers. *Optics Letters*, 20(20):2093–2095, 1995.

[21] M. L. Gorodetsky and V. S. Ilchenko. Optical microsphere resonators: Optimal coupling to high Q whispering gallery modes. *OSA:B*, 16(1):147–154, January 1999.

[22] S. C. Greedy, S. V. Boriskina, P. Sewell, and T. M. Benson. Design and simulation tools for optical microresonators. In Giancarlo C. Righini and Seppo Honkanen, editors, *Integrated optics devices V, Proceedings of SPIE*, volume 4277, pages 21–32, 2001.

[23] R. Grover, P. P. Absil, V. Van, Hryniewicz J. V., B. E. Little, O. King, L. C. Calhoun, F. G. Johnson, and P. T. Ho. Vertically coupled GaInAsP-InP microring resonator. *Optics Letters*, 26(8):506–508, 2001.

[24] S. C. Hagness, D. Rafizadeh, S. T. Ho, and A. Taflove. FDTD microcavity simulations: Design and experimental realization of waveguide coupled single mode ring and whispering gallery mode disk resonator. *IEEE J. Lightwave Technology*, 15(11):2154–2165, November 1997.

[25] Manfred Hammer. Coupled mode model for 3D directional couplers. NAIS project, Internal document.

[26] Manfred Hammer. Standard ringresonator model. NAIS project, Internal document.

[27] Hermann A Haus. *Waves and Fields in Optoelectronics*. Prentice Hall, 1984.

[28] G. L. Hower, R. G. Olsen, J. D. Earls, and J. B. Schneider. Inaccuracies in numerical calculation of scattering near natural frequencies of penetrable objects. *IEEE Trans. Antennas Propagation*, 41(7):982–986, July 1993.

[29] H. Ishikawa, H. Tamaru, and K. Miyano. Optical coupling between a microresonator and an adjacent dielectric structure: effects of resonator size. *J. Opt. Soc. Am. B*, 18(8):762–765, 2001.

[30] Sangin Kim and A. Gopinath. Vector analysis of optical dielectric waveguide bends using finite-difference method. *JLT*, 1996.

[31] D. J. W. Klunder, M. L. M. Balistreri, F. C. Blom, H. W. J. M. Hoekstra, A. Driessen, L. Kuipers, and N. F. van Hulst. Detailed analysis of the intracavity phenomena inside a cylindrical microresonator. *IEEE J. Lightwave Technology*, 20(3):519–529, 2002.

[32] D. J. W. Klunder, E. Krioukov, F. S. Tan, T van der Veen, H. F. Bulthuis, G. Sengo, C. Otto, H. W. J. M. Hoekstra, and A. Driessen. Vertically and laterally waveguide-coupled cylindrical microresonators in Si_3N_4 on SiO_2 technology. *Appl. Phys. B*, 73:603–608, 2001.

[33] D.J.W. Klunder, M.L.M. Balisteri, F.C. Blom, J.W.M. Hoekstra, A. Driessen, L. Kuipers, and N.F. Van Hulst. High-resolution photon-scanning tunneling microscope measurements of the whispering gallery modes in a cylindrical microresonator. *IEEE Photonics Technology Letters*, 12(11):1531–1533, November 2000.

[34] Y. Kokubun, S. Kubota, and S. T. Chu. Polarization independent vertically coupled microring resonator filter. *Electronics Letters*, 37(2), January 2001.

[35] J. Krupka, D. Cros, M. Aubourg, and P. Guillon. Study of whispering gallery modes in anisotropic single-crystal dielectric resonators. *IEEE Trans. Microwave Theory and Techniques*, 42(1):56–61, January 1994.

[36] A. F. J. Levi, R. E. Slusher, S. L. McCall, J. L. Glass, S. J. Pearton, and R. A. Logan. Directional light coupling from microdisk laser. *Applied Physics Letter*, 62:561–563, 1993.

[37] Bing-Jing Li and Pao-Lo Liu. Numerical analysis of the whispering gallery modes by finite difference time domain methods. *IEEE J. Quantum Electronics*, 32(9):1583–1587, September 1996.

[38] B. E. Little, S. T. Chu, H. A. Haus, J. Foresi, and J. P. Laine. Microring resonator channel dropping filters. *IEEE J. Lightwave Technology*, 15:998–1005, 1997.

[39] B. E. Little, Sai T. Chu, J. V. Hryniewicz, and P. P. Absil. Filter synthesis for periodically coupled microring resonators. *Optics Letters*, 25(5):344–346, 2000.

[40] B. E. Little, J. P. Laine, and H. A. Haus. Analytic theory of coupling from tapered fibers and half blocks into microsphere resonators. *IEEE J. Lightwave Technology*, 17(4):704–715, April 1999.

[41] Bin Liu, Shakouri Ali, and J. E. Bowers. Passive microring resonator coupled lasers. *Applied Physics Letters*, 79(22):3561–3563, 2001.

[42] W. W. Lui, C. L. Xu, T. Hirono, K. Yokoyama, and Wei-Ping Huang. Full-vectorial wave propagation in semiconductor optical bending waveguides and equivalent straight waveguide approximations. *IEEE J. Lightwave Technology*, 16(5):910–914, May 1998.

[43] C. Manolatou, M. J. Khan, S. Fan, P. R. Villeneuve, H. A. Haus, and J. D. Joannopoulos. Coupling of modes analysis of resonant channel add drop filters. *IEEE J. Quantum Electronics*, 35(9):1322–1331, September 1999.

[44] E. A. J. Marcatili. Bends in optical dielectric guides. *The Bell System Technical Journal*, September:2103–2132, 1969.

[45] D Marcuse. Bending losses of the asymmetric slab waveguide. *The Bell System Technical Journal*, October:2551–2563, 1971.

[46] K. Okamoto. *Fundamentals of Optical Waveguides*. Academic Press, 2000.

[47] J. H. Richmond. Scattering by a dielectric cylinder of arbitrary cross section shape. *IEEE Trans. Antennas Propagation*, 13:334–341, May 1965.

[48] D. R. Rowland and J. D. Love. Evanescent wave coupling of whispering gallery modes of a dielectric cylinder. *IEE Proceedings-J*, 140(3):177–188, 1993.

[49] L. F. Stokes, M. Chodorow, and Shaw H. J. All single mode fiber resonator. *Optics Letters*, 7(6):288–290, June 1982.

[50] T Tamir (Ed.). *Integrated Optics (Second Corrected and Updated Edition)*. Springer-Verlag, Germany, 1982.

[51] V. Van, P.P. Absil, J. V. Hryniewicz, and P. T. Ho. Propagation loss in single-mode GaAs-AlGaAs microring resonators: measurement and model. *IEEE J. Lightwave Technology*, 19(11):1734–1739, 2001.

[52] V. Van, T. A. Ibrahim, P. P. Absil, F. G. Johnson, R. Grover, and P.T. Ho. Optical signal processing using nonlinear semiconductor microring resonators. *IEEE J. of Selected Topics in Quantum Electronics*, 8(3):705–713, 2002.

[53] C. Vassallo. *Optical Waveguide Concepts*. Elsevier, Amsterdam, 1991.

[54] A. Yariv. Universal relations for coupling of optical power between microresonators and dielectric waveguides. *Electronics Letters*, 36(4), 2000.

[55] A. Yariv. Critical coupling and its control in optical waveguide-ring resonator systems. *IEEE Photonics Technology Letters*, 14(4):483–485, April 2002.

[56] K. C. Zeng, L. Dai, J. Y. Lin, and H. X. Jiang. Optical resonance modes in InGaN/GaN multiple quantum well microring cavities. *Applied Physics Letters*, 75(17):2563–2565, 1999.